

AD 669252

A FIELD-EMISSION MICROSCOPE INVESTIGATION OF THE EFFECTS  
OF AMBIENT ATMOSPHERES ON THE STRESS-CORROSION CRACKING  
OF URANIUM-MOLYBDENUM ALLOYS

FINAL REPORT

S. A. Hoenig  
Principal Investigator

and

H. Suisona  
Research Associate



B

United States Army Terminal Ballistics Laboratory  
Ballistic Research Laboratory  
Aberdeen Proving Ground  
Aberdeen, Maryland

Contract No. DA-18-001-AMC-1063 (x)

This document has been approved for public release and sale;  
its distribution is unlimited.



ENGINEERING EXPERIMENT STATION  
COLLEGE OF ENGINEERING  
THE UNIVERSITY OF ARIZONA  
TUCSON, ARIZONA

Reproduced by the  
CLEARINGHOUSE  
for Federal Scientific & Technical  
Information Springfield Va. 22151

128

**A FIELD-EMISSION MICROSCOPE INVESTIGATION OF THE EFFECTS  
OF AMBIENT ATMOSPHERES ON THE STRESS-CORROSION CRACKING  
OF URANIUM-MOLYBDENUM ALLOYS**

**FINAL REPORT**

**S. A. Hoenig  
Principal Investigator**

**and**

**H. Sulsona  
Research Associate**

**This document has been approved for public release and sale;  
its distribution is unlimited.**

**9 March 1968**

**United States Army Terminal Ballistics Laboratory  
Ballistic Research Laboratory  
Aberdeen Proving Ground  
Aberdeen, Maryland**

**Contract No. DA-18-001-AMC-1063 (x)**

**Department of Electrical Engineering  
College of Engineering  
The University of Arizona  
Tucson, Arizona 85721**

## TABLE OF CONTENTS

Chapter	Page
LIST OF ILLUSTRATIONS.....	vii
LIST OF TABLES.....	ix
ABSTRACT.....	x
I. INTRODUCTION.....	1
1.1 General Remarks.....	1
1.2 The Problem.....	3
II. STRESS-CORROSION CRACKING.....	5
2.1 Definition of Stress-Corrosion Cracking.....	5
2.2 Theories of Stress-Corrosion Cracking.....	7
2.2.1 The Electrochemical and Chemical Theories.....	7
2.2.2 The Mechanical Theory.....	11
2.2.3 The Electrochemical-Mechanical Theory.....	13
2.2.4 The Surface-Energy Theory.....	16
2.3 Hydrogen Embrittlement.....	17
2.4 Classical Examples of Stress-Corrosion Cracking..	19
2.4.1 Cu-Zn Alloys.....	19
2.4.2 Iron Alloys.....	20
2.4.3 Aluminum Alloys.....	21
2.4.4 Titanium Alloys.....	21
2.5 General Approach to the Stress-Corrosion Cracking Problem by Other Researchers.....	22
2.6 Summary.....	22
III. FRACTURE.....	24
3.1 Introduction.....	24
3.2 Brittle Fracture.....	25
3.2.1 Crack Nucleation and Propagation.....	28
3.3 Ductile Fracture.....	29
3.4 Cracking Susceptibility in Stress-Corrosion Cracking.....	30
3.5 Intergranular and Transgranular Cracking.....	33

TABLE OF CONTENTS--Continued

Chapter	Page
IV. STRESS-CORROSION CRACKING IN URANIUM-MOLYBDENUM ALLOYS.....	36
4.1 Introductory Remarks.....	36
4.2 Work by Other Researchers.....	36
4.2.1 Mode of Cracking.....	38
4.2.2 Agent or Agents Responsible for Stress- Corrosion Cracking.....	39
4.2.3 Possible Protection Techniques.....	39
4.3 General Characteristics of Uranium-Molybdenum Alloys for Reactor Applications.....	41
4.3.1 Phases Encountered in Uranium Alloys.....	41
4.3.2 General Characteristics of U-10 <sup>W</sup> /o Mo for Reactor Applications.....	43
4.4 Summary.....	44
V. RESEARCH EFFORT AT THE UNIVERSITY OF ARIZONA.....	45
5.1 Initial Considerations.....	45
5.2 Experimental Apparatus and Techniques.....	47
5.2.1 Apparatus.....	47
5.2.2 Experimental Techniques.....	53
VI. EXPERIMENTAL RESULTS.....	62
6.1 General.....	62
6.2 Tests in the Field-Emission Microscope.....	62
6.2.1 Thermal Etching.....	62
6.2.2 Dry Tests.....	63
6.2.3 Wet Tests.....	66
6.2.4 Time-to-Fail Tests.....	68
6.3 Cathodic Protection and Effect of Electric Fields.....	69
6.4 Cyclic-Loading Tests.....	70
6.5 Summary.....	71
VII. DISCUSSION AND CONCLUSIONS.....	72
7.1 Tests in the Field-Emission Microscope.....	72
7.1.1 Heat Treatment - Critical Stress.....	72
7.1.2 Dry Tests.....	73
7.1.3 Wet Tests.....	75
7.2 Cathodic Protection and Electric Fields.....	76
7.3 Dry Nitrogen as a Protective Shield.....	77
7.4 Design Considerations.....	77
7.5 Conclusions.....	77

TABLL OF CONTENTS--Continued

Chap'	Page
VIII. RECOMMENDATIONS FOR FUTURE RESEARCHi.....	80
8.1 Alpha-Phase Precipitation.....	80
8.2 Corrosion Studies.....	80
8.3 Electropolishing and Hydrogen Pick-up.....	81
8.4 Shot Peening.....	81
8.5 Effect of Inert Atmospheres.....	82
APPENDIX A.....	83
Partial Dislocations and the Stacking Fault.....	83
REFERENCES.....	111

LIST OF ILLUSTRATIONS

No.		Page
1	Stages in the re-initiation of a crack from a slip band ..	93
2	Dislocation mechanisms of crack nucleation .....	94
3	(a) Equilibrium diagram of the uranium-molybdenum alloy system; (b) TTT diagram of a U-2.5 <sup>W/o</sup> Mo alloy as determined by metallography and hardness tests .....	95
4	Cylindrical field-emission microscope for wire studies ...	96
5	Modified Field-Emission Microscope pulling assembly; gas mixing chamber and gas washer tank .....	97
6	Cathodic protection apparatus and electric circuit .....	98
7	Static, electric fields apparatus and electric circuit . .	99
8	Cyclic-loading apparatus .....	100
9	Thermal grooving and etch pits in a U-10 <sup>W/o</sup> Mo specimen (400X) .....	101
10	Slip bands and microcracks in a U-10 <sup>W/o</sup> Mo specimen exposed to pure, dry oxygen for 24 hours (600X) .....	101
11	Coalescence of slip bands generating microcracks .....	102
12	Intergranular cracks in a U-10 <sup>W/o</sup> Mo specimen exposed to pure, dry oxygen for 24 hours (800X) .....	103
13	Surface deterioration of a U-10 <sup>W/o</sup> Mo specimen exposed to wet oxygen (.6 normalized partial pressure) (400X) .....	103
14	Intersection of slip bands and concentration of corrosion products on a U-10 <sup>W/o</sup> Mo specimen exposed to wet oxygen (.6 normalized partial pressure) (600X) .....	104
15	Intergranular and transgranular cracks on a U-10 <sup>W/o</sup> Mo specimen exposed to wet oxygen (.6 normalized partial pressure (600X) .....	104

LIST OF ILLUSTRATIONS--Continued

No.		Page
16	Load vs. time to fail of U-10 <sup>w/o</sup> Mo specimens, "as-received" and heat treated .....	105
17	Normalized partial pressure of water vapor vs. time to fail with tensile stress as a parameter .....	106
18	Load vs. time to fail for U-10 <sup>w/o</sup> Mo specimens exposed to hydrogen both dry and saturated with water vapor at room temperature .....	107
19	Sequence of photomicrographs showing the process of fracture in a cyclically loaded specimen at intervals of 10 cycles. Specimen was loaded in dry, laboratory air ...	108
20	A total dislocation (edge orientation) in a face-centered cubic lattice as viewed when looking down on the slip plane, after Reed-Hill .....	109
21	Partial dislocation in a face-centered cubic lattice, after Reed-Hill .....	109
22	An extended dislocation, after Reed-Hill .....	110
23	The (1 $\bar{1}$ 0) plane of the bcc lattice, after Weertman .....	110

LIST OF TABLES

Table		Page
I	DRY TESTS .....	88
II	WET TESTS .....	90
III	CYCLIC-LOADING TESTS .....	91

## ABSTRACT

The effects of heat treatment and ambient atmospheres on the stress-corrosion cracking behavior of U-10<sup>W</sup>/o Mo were investigated using a field-emission microscope of cylindrical geometry. Cathodic protection and the effect of static electric DC fields were investigated as possible protective techniques in the stress-corrosion cracking of U-10<sup>W</sup>/o Mo. A special "gas shield" protective technique was also investigated.

The stress-corrosion cracking behavior of U-10<sup>W</sup>/o Mo was found to be influenced by heat treatments. A gamma homogenization and quench followed by a tempering treatment were found to be most beneficial in reducing the susceptibility of the alloy.

A tentative "critical stress" for initiation of stress-corrosion cracking was set at 36,500 psi. This critical stress was found to be strongly dependent upon heat treatments and internal structure.

Cracking of U-10<sup>W</sup>/o Mo in specific atmospheres was found to be either intergranular, transgranular or both, depending on the particular atmosphere. Intergranular cracking was found to be caused by pure, dry oxygen, while transgranular cracking was found to be promoted by increasing the water vapor content of the atmosphere.

U-10<sup>W</sup>/o Mo was found to be susceptible to hydrogen embrittlement.

Cathodic protection and electric fields had no effect on the stress-corrosion cracking behavior of U-10<sup>W</sup>/o Mo. Pure, dry nitrogen

on the other hand, was found to be most effective as a protective shield during cyclic loading of U-10<sup>w</sup>/o Mo specimens.

## CHAPTER I

### INTRODUCTION

#### 1.1 General Remarks

Since the first nuclear reactor became critical in 1942, the number and types of reactors have multiplied many times. The degree of sophistication which reactor design has achieved was undreamed of in 1942.

Among the different types of reactors which present-day technology has produced, the research reactor plays a very important role. In an effort to obtain the maximum benefit from research programs, research reactors have been developed with a diversity of shapes, forms, and structural characteristics. The development of these reactors has produced some very strange names, to wit, Super Kukla, Godiva, and Godiva II.

The reactors named above are part of a sophisticated group of small, bare, unmoderated reactors, some of which use highly enriched uranium alloyed with 10 percent by weight of molybdenum as the fuel material (1).

The addition of molybdenum to the uranium enhances the high-temperature characteristics of the fuel, by improving the dimensional stability of uranium under thermal cycling. Furthermore, adding molybdenum to uranium reduces the thermal expansion stresses because of a lower modulus of elasticity in the resulting alloy.

A U-10<sup>w</sup>/o Mo alloy was used at the Lawrence Radiation Laboratory (2) as fuel and structural material in its Kukla fast-burst reactor. The alloy and, in particular, the bolts which hold the reactor core have been plagued with unexplained cracking during and after fabrication. The bolts failed after their insertion in the reactor, before the reactor was operated.

A number of tests were conducted in an effort to explain and prevent this behavior. The conclusions (3) were that failure was caused by stress-corrosion cracking of the alloy. Furthermore, it was reported (3) that atmospheric oxygen was believed to be responsible for the stress-corrosion cracking.

Stress-corrosion cracking is defined as early, brittle failure of usually ductile materials when subjected to tensile stresses in the presence of a particular corrosive environment.

It was not possible, by means of the tests mentioned above, to determine the nature and extent of cracking and the effect on this cracking of such parameters as stress levels, strain rate, and gas concentrations.

In 1965, the Ballistics Research Laboratory of the United States Army at Aberdeen, Maryland, began a reactor research program in which it was planned to use a bare-type reactor using U-10<sup>w</sup>/o Mo as fuel and structural material. In the light of past experience with similar reactors, it was decided that the stress-corrosion cracking behavior of the highly desirable alloy (U-10<sup>w</sup>/o Mo) should be investigated further in an effort to determine the feasibility of improving its behavior or to justify a research program for a new alloy.

A research contract was set up in June of 1966 between the United States Army and the University of Arizona in which it was agreed that the University of Arizona would investigate the stress-corrosion cracking behavior of the U-10<sup>W</sup>/o Mo alloy using a field-emission microscope of cylindrical geometry (4, 5) as the principal tool of research. The United States Army would provide the specimens in the form of thin wires. The contract was funded as contract No. DA-18-001-AMC-1063(x) and covered the period 1 June 1966 to 31 August 1967.

#### 1.2 The Problem

The above-described observations indicated U-10<sup>W</sup>/o Mo alloys, of reasonable strength and satisfactory ductility, to be susceptible to early, brittle failure when loaded in tension in the presence of atmospheric air. All of the failure characteristics reported in the literature pointed toward stress-corrosion cracking.

The problem at hand, therefore, has been to extend the understanding of the stress-corrosion cracking of this particular alloy by conducting an investigation of the following:

- a. The mode of fracture, i.e., whether it is intergranular or transgranular.
- b. The agent or agents responsible for the stress-corrosion cracking of the alloy.
- c. The effect of stress levels.

The above aspects of behavior of the U-10<sup>W</sup>/o Mo alloy have been studied with the aid of a field-emission microscope of cylindrical geometry as the principal tool of research.

The relative importance of the above factors will be evaluated in the chapters which follow, preceded by a discussion of stress-corrosion cracking and fracture as they pertain to this work.

## CHAPTER II

### STRESS-CORROSION CRACKING

#### 2.1 Definition of Stress-Corrosion Cracking

The phenomenon of stress-corrosion cracking is well known in metallurgy. It illustrates very clearly the interplay of metallurgical and chemical factors in the failure of an engineering material. Stress-corrosion cracking is generally the cause of failure whenever alloys of high strength and sufficient ductility fail catastrophically by cracking when stressed in tension in particular environments. Residual cooling stresses are often sufficient to cause stress-corrosion cracking (6, 7). The agents responsible for weakening the metal structure and grain boundaries are specific to each metal and fortunately few in number.

Stress-corrosion cracking is characterized by profuse cracking of a metal structure. Cracks originate on the surface of the metal and propagate into the structure along specific paths which depend on the alloy system and the particular corrodent. When the cracks follow grain boundaries, cracking is known as intergranular. All other paths are termed transgranular. A treatment of these modes of crack propagation will be presented in Chapter III.

Ultra-pure metals do not suffer stress-corrosion cracking in any environment (8), even though instances are found in the literature which report the stress-corrosion cracking of high-purity metals.

For example, Perryman (9) refers to the cracking of high-purity manganese in distilled water. In this case, some minor impurity may be responsible for this behavior. This would be particularly true of service at elevated temperatures in which temperature-diffused impurities may be responsible for imparting stress-corrosion cracking susceptibility to otherwise ultra-pure metals.

Impurities may or may not be involved in the stress-corrosion cracking of alloys. Interstitial nitrogen, for example, is important in imparting susceptibility to stress-corrosion cracking in austenitic stainless steels (10). On the other hand, brass, Cu-Au, Ag-Au, and Mg-Al alloys suffer stress-corrosion cracking when exposed to certain corrodents, even when the alloy is of the highest purity (8).

The corrosion phenomena accompanying stress-corrosion cracking are not simple. The chemical agents and modes of fracture and corrosion are far too varied to classify in a simple way. There is, however, a classification offered by Parkins (11) based on the type of cracking which is observed. He suggests that in stress-corrosion cracking phenomena there exists a series of fracture modes which ranges from transgranular to intergranular, depending on the alloy, its thermal history, and the specific corrosive environment. This classification has been used by other workers (8, 9, 12) to systematize their results. It will be used in this work also.

The essential requirement of tensile stresses (residual, applied, or both) in stress-corrosion cracking adds to the complexity of the problem. A structural metal, fully annealed and free from applied

stresses, can sometimes exist in harmony with otherwise damaging chemical agents with no more observable attack than superficial corrosion of the surface. Furthermore, if the stresses are compressive rather than tensile, the metal will support the load without cracking (8).

The complex behavior of stress-corrosion cracking phenomena is further enhanced by the fact that in stress-corrosion cracking a metal fails at stress levels considerably lower than are required for purely mechanical failure alone. These stress levels are usually within 20 to 30 per cent of the yield strength. Time to fail is considerably shorter than would be required if purely corrosive mechanisms were responsible for the failure of the metal.

In trying to explain stress-corrosion cracking, several theories have been proposed (13). These theories are the result of the modifications and combinations of two basic mechanisms: a purely electrochemical mechanism and a purely mechanical mechanism. The stress-corrosion cracking theories can be classified into four major groups: 1. the electrochemical-chemical theory; 2. the mechanical theory; 3. the electrochemical-mechanical theory; and 4. the surface energy theory. These will be discussed below.

## 2.2 Theories of Stress-Corrosion Cracking

### 2.2.1 The Electrochemical and Chemical Theories

A. The Electrochemical Theory. Many of the stress-corrosion cracking phenomena can be explained by an electrochemical mechanism.

The electrochemical theory is based on the assumption that the alloy susceptible to stress-corrosion cracking suffers corrosion along more or less continuous paths which start on the surface and penetrate the bulk of the metal. These paths are believed to be the results of micro-segregation and subsequent coalescence of solute atoms and impurities and are considered to be anodic with respect to the surrounding metal (14).

Electrochemical potential measurements of preferred stress-corrosion paths have indeed shown these paths to be anodic to the rest of the grain (15). Anodic grain boundaries, in solutions that cause stress-corrosion cracking, have been demonstrated for brass in oxygenated ammonia by Mears, Brown, and Dix (16), and Bakish and Robertson (17).

Metal along the anodic paths tends to dissolve forming a sharp groove at which stress is concentrated and plastic deformation is accentuated. The groove gradually widens, and the groove root tends to establish the thermodynamic, dihedral angle  $\theta$  given by

$$\cos \theta/2 = \gamma_B/2\gamma_S$$

where  $\gamma_B$  is the boundary energy or surface tension, and  $\gamma_S$  is the surface energy of the metal-corrodent interface. When this angle is established, the electrode potential at the groove becomes equal to that at the undisturbed metal-corrodent interface. The metal surface between these two points dissolves and changes contour upsetting the equilibrium angle. The groove then deepens to restore the equilibrium angle.

In addition to electrochemical action, the electrochemical theory requires that a localized, sustained tensile stress act in a direction tending to pull the metal apart perpendicular to the anodic path (18). The ultimate effect of this stress is to expose fresh metal to the corrodent.

Under chemical attack, a film of corrosion products forms over the surface of the metal. This film can be either protective or non-protective. A protective film guards the metal matrix against further corrosive action. Such a film can be protective only when its structure corresponds to the structure of the underlying crystals, or if it is maintained intact and continuous (19). Stress concentrations at the root of an existing crack, however, strain the metal beyond the yield point and break any protective oxide film that may have formed exposing fresh anodic metal to the corrosive environment (20).

Logan (14) suggests that there exist stress concentrations at the root of locally corroded areas and at sufficient concentrations of stress, the metal might start to tear by mechanical action. This mechanical tearing would also expose fresh metal to the corrodent, and the stress-corrosion process would continue.

Not all corrosive phenomena involve a wet or humid environment. Dry corrosion or gaseous corrosion involves the physical and chemical interaction between gases and metals. A complete treatment of gas-metal surface interactions is beyond the scope of this work. A few pertinent comments, however, will be made in the following section.

B. The Chemical Theory. Dry corrosion occurs mainly through the chemical reaction of gases with metal or alloy surfaces. When a completely clean, oxide-free surface of metal is exposed to oxygen, for instance, an instantaneous adsorption of gas takes place on the metal surface. This adsorption is thought to be the result of secondary attraction forces between the surface atoms of the metal and the oxygen molecules. This adsorption is purely physical in nature; the secondary attraction forces are thought to be due to the residual valency of the surface atoms of the metal and the oxygen molecules.

In the second stage the oxygen gradually enters into combination with the metal by electron transfer or electron sharing between oxygen and metal atoms. This type of adsorption is known as chemisorption and involves forces of a chemical nature. In order that gas molecules may enter into such combination with metals, they may first dissociate into atoms or ions. The dissociation requires a certain amount of energy which can be supplied either because of chemical affinity of a gas for the metal or by the heat of adsorption.

After the surface of the metal becomes covered with a monolayer of oxide, the growth of the film perpendicular to the metal surface commences, and this may result in the formation of a thick oxide layer or scale. Once the thick oxide layer is formed, a mechanism involving stress concentration and oxide film rupture can be invoked to explain the exposure of fresh metal to the corrodent. Stress-corrosion cracking would then proceed as explained in previous paragraphs.

For a more extensive treatment of chemisorption and gas-surface interactions the reader is referred to works by Ehrlich (21) and by Huang (22).

The electrochemical-chemical theory fails to account for the highly specific effects of certain chemical agents in causing failure where plastic deformation accompanying cold work or creep precedes crack formation. Anodic and cathodic areas within a metal should react to any electrolyte or chemical agent, not just a few.

Summarizing, then, the electrochemical-chemical theory proposes that crack initiation and propagation are due entirely to an electrochemical or chemical mechanism with physical stresses playing only a minor role, that of assisting in the exposure of fresh metal to the corrodent.

### 2.2.2 The Mechanical Theory

The mechanical theory of stress-corrosion cracking completely interchanges the importance of the roles played by chemical and physical factors in the failure mechanism (13). In this theory, regions of high stress concentration, due to dislocation pile-ups and pinned dislocations, are assisted by the chemical action of the corrodent in causing early failure of the metal.

A period of "incubation" has been observed prior to crack formation in most alloys susceptible to stress-corrosion cracking. Haynie et al. (13) suggest that since the length of the "incubation" period prior to crack formation is strongly stress dependent, the motion of dislocations may be involved. Dislocations may pile

up along slip planes at free surfaces. The high stresses associated with these pile-ups should eventually exceed the forces associated with the free surface (see "The Surface Energy Theory" below) and cause coarse slip. Coarse slip has been correlated with the breakdown of protective oxides and the initiation of transcrystalline stress-corrosion cracking (23).

The mechanical theory of stress-corrosion cracking requires that a crack propagate through ductile material (a material capable of appreciable plastic flow) by a purely mechanical mechanism. In a ductile material, the stress concentration at the root of the crack is lowered by local yielding of the material to form a greater root radius. Therefore, the material at the root of a crack must be embrittled before the crack can propagate by a purely mechanical mechanism.

Several embrittling mechanisms have been proposed, all of which involve the stopping of dislocations and straining of the crystalline lattice. Dislocation interactions will be discussed in Chapter III, and hydrogen embrittlement will be the subject of a section below.

The mechanical theory of stress-corrosion cracking is inconsistent with several observed characteristics of stress-corrosion cracking. The most outstanding inconsistency is that in many susceptible alloy systems stress-corrosion cracking can be accelerated or stopped by anodic and cathodic currents, respectively (13). This obviously suggests an electrochemical dependence of stress-corrosion cracking.

Another drawback of the mechanical theory is that the cracking and failure rates which have been observed in stress-corrosion cracking are much slower than they would be if only a mechanical mechanism were operative.

### 2.2.3 The Electrochemical-Mechanical Theory

The electrochemical-mechanical theory is a combination of the two theories discussed above. This theory suggests that, in a metal, regions of high stress concentration due to dislocation pile-ups promote enhanced corrosive activity or chemical attack. This enhanced corrosive activity is conducive to crack propagation. Cracks are thought to be nucleated through dislocation interactions and dislocation coalescence (see Chapter III). The cracks then propagate in a step-like manner in bursts of brittle fracture.

Many investigators (12, 13, 24) have observed alternating slow and fast crack propagation rates. These alternating rates are assumed to be due to electrochemical or chemical and mechanical mechanisms, respectively.

Forty (24) has proposed a stress-corrosion cracking mechanism in which the metal at the surface of a specimen or around the tip of an established crack becomes embrittled as a result of exposure to the chemical environment. The so-called embrittled zone sufficiently restricts plastic deformation to allow a crack to be formed or an established crack to penetrate the normal metal. The penetration will continue into the metal provided the crack acquires a sufficient velocity and does not encounter an abnormally soft region such as a

pre-existing slip band (24) (see Fig. 1). In this model, subsequent propagation of the stopped crack would make use of a repetition of the mechanism proposed by Forty (24) which is described in Fig. 1.

Slip bands are normally hard regions which result from plastic flow and work hardening. Therefore, the statement made above of a "soft, pre-existing slip band" must be qualified. Consider the short-range ordered regions in certain solid solution alloys. These regions are known to be hard (24). Consider now the passage of one dislocation through this ordered region. The first dislocation destroys the local order (10, 24) thereby softening the region. The trace of this dislocation, and that of the next few, produces a "soft" slip band where, according to Forty (24), a crack can be stopped. Passage of many dislocations through this region will eventually restore the order and the locally hardened condition. This softening-hardening mechanism can, in theory, be repeated over and over allowing a crack to propagate in a step-like manner.

Barnartt (15) suggests that crack propagation occurs as alternating steps of slow anodic attack resulting in little crack extension and of sudden fracture resulting in a greater, but still microscopic, extension step. He further proposes that the over-all propagation rate may be increased by increasing the length of each brittle step or the rate of the re-initiation process. The re-initiation process need not be the same as the original crack nucleation process. Crack nucleation as a result of dislocation interactions will be treated in Chapter III.

The enhanced corrosive activity proposed in the electrochemical-mechanical theory may be understood in terms of Uhlig's (8) postulate which states that certain ions selectively adsorbed at metallurgical imperfections weaken the attraction between the metal atoms causing easy rupture of the metal bonds. Bergen (25) suggests a diffusion mechanism to explain the movement of these ions to the regions of highest tensile stress. He notes that the specific ions responsible for complex corrosion behavior are relatively large. Within an oxide or corrosion film, and in the presence of tensile stresses, differences in the sizes of the ions will result in motion of the larger ions to areas of high tensile stress. Motion of the larger ions to areas of high tensile stress might be expected because this would reduce the Gibbs free energy, in agreement with classical diffusion theory. Bergen (25) further postulates that when the migrating ions arrive at the points of high tensile stress, concentration effects or hydrolysis effects may result in a rather large increase in corrosion tendencies. This locally corrosive environment favors dissolution and degeneration of the metal. Thomas and Allio (26) have observed the migration of chloride ions, under tensile stresses, in the oxide of Type 304 stainless steel. They have further observed that this migration is reversible if the stresses are removed.

The electrochemical-mechanical theory is currently favored by most researchers (13, 26) and seems to agree with most stress-corrosion cracking observations.

#### 2.2.4 The Surface-Energy Theory

The surface-energy theory is based on the Griffith crack mechanism for brittle fracture (27). The Griffith theory of brittle fracture will be discussed in some detail in Chapter III. Here it may suffice to say that the Griffith theory presupposes the existence of microcracks in a material which fractures in a brittle manner. While there is no reliable evidence that Griffith cracks exist in unstressed metals (13), it is known that plastic deformation can nucleate microcracks (28, 29, 30). Griffith's theory suggests that the work done in extending a pre-existing crack is expended in the creation of two new surfaces.

An extension of the concept of surface tension for liquids (31) has led to the definition of a "free surface energy" for solids. The work required to extend a surface by a unit of area is called the "free surface energy" (31). In the solution of problems involving surfaces, very often a hypothetical surface tension is substituted for the free energy. This tension is assumed to act in all directions parallel to the surface and is equal to the free surface energy (31, 32). The work done per unit area in extending a surface which is pulling, or is being pulled, with a tension of  $\gamma$  dynes/cm will be  $\gamma$  ergs/cm<sup>2</sup> and is equal to the free surface energy (32).

The surface energy theory proposes that certain selectively adsorbed ions locally lower the surface energy. The lower surface energy should permit crack propagation at stress levels considerably below those stresses required in the absence of the adsorbed ions.

While surface energy lowering may contribute to stress-corrosion cracking, the available data are conflicting (13, 33); surface energy lowering alone is certainly not responsible for stress-corrosion cracking.

An interesting phenomenon which is often mistaken for stress-corrosion cracking is hydrogen-stress cracking produced by hydrogen embrittlement. The following section treats the current theories of hydrogen embrittlement.

### 2.3 Hydrogen Embrittlement

Hydrogen embrittlement of a susceptible specimen, in laboratory testing, is characterized by a decrease in tensile ductility (reduction in area) in a tensile test, by a decrease in notch tensile strength, and by delayed failure in a static loading test. Usually, the yield strengths of the specimens are relatively unaffected (34).

Hydrogen may be introduced into susceptible materials in a variety of ways. Introduction may be the result of localized electrolytic reactions within the metal in strongly acidic ( $\text{pH} < 4$ ) or strongly alkaline ( $\text{pH} > 10$ ) solutions. In either case, hydrogen ions are reduced to hydrogen atoms at the local cathode (34). Hydrogen may be retained during electroplating operations (35), it may be retained during solidification of castings (36), or generated during corrosion processes in the presence of water vapor (37, 38).

Several theories have been proposed to explain the mechanism of hydrogen embrittlement. Basically, however, the theories fall into

two groups: the "pressure theory" (39, 40) and the "decreasing-strength theory" (41, 42).

The pressure theory proposes that hydrogen embrittlement results from the precipitation of hydrogen gas at defects such as inclusions and expansion of microcracks and voids due to the gas pressure. In this model, the internal pressure lowers the applied stress necessary to cause crack growth.

The decreasing-strength theory, on the other hand, proposes that the presence of dissolved hydrogen lowers the cohesive strength of the lattice. This decrease in cohesive strength results in a decrease in the surface energy of fracture and, hence, in a lowering of the applied stress necessary for crack propagation.

Since both models predict a lowering in the stress required for crack propagation, it is very difficult to separate them experimentally.

It is extremely difficult to determine whether fracture in some corrosive environments was the result of hydrogen embrittlement or stress-corrosion cracking since the fracture surfaces in many instances exhibit many similar features. In high-strength steels, for instance, both modes of failure are predominantly intergranular (43); whereas in other alloys they can be either intergranular or transgranular or both.

Electron microscope studies have revealed that stress-corrosion cracks nucleate at the surface, whereas hydrogen-corrosion cracks

nucleate beneath the surface (34). In addition, the fracture surfaces resulting from stress-corrosion cracking tend to be smoother and exhibit fewer hairline cracks than those resulting from hydrogen embrittlement. However, corrosion products in both cases tend to obscure the details, and the exact analysis in all situations is extremely difficult (34).

Objections to both theories of hydrogen embrittlement have been raised by workers in the field. A discussion of these objections is beyond the scope of this treatment. The reader is referred to excellent treatments by Tetelman (34, 39, 40) for additional information on this subject.

## 2.4 Classical Examples of Stress-Corrosion Cracking

### 2.4.1 Cu-Zn Alloys

The oldest example of stress-corrosion cracking known to man is that exhibited by the very useful Cu-Zn alloys, in particular, the alpha brasses. Alpha brasses are susceptible to stress-corrosion cracking in atmospheres containing ammonia or amines, or when in contact with mercury vapor (44).

It has been suggested (45) that both oxygen and moisture are needed to make ammonia corrosive. Moisture films on a metal surface may concentrate significant quantities of ammonia from atmospheres that are low in ammonia concentration. This in turn would increase the ammonia on the surface by a large factor, and electro-chemical action might take place at the grain boundaries (46) which are considered anodic with respect to the bulk of the grain (16). This suggests

that stress-corrosion cracking of Cu-Zn alloys in ammoniacal atmospheres is primarily intergranular, in agreement with experimental observations (16, 46). Stress-corrosion cracking of Cu-Zn alloys caused by mercury vapor is somewhat more complicated and will not be discussed here.

#### 2.4.2 Iron Alloys

Iron alloys, particularly high-strength steels, precipitation hardenable steels, and some austenitic stainless steels, are susceptible to stress-corrosion cracking and hydrogen embrittlement (47). It appears as though any substance or environment bearing the chloride ion is capable of causing stress-corrosion cracking in iron alloys (26, 48).

The stress-corrosion cracking of iron alloys is complicated by the fact that the fracture parameters vary from grade to grade of steel and from heat to heat of the same grade (48).

The stress-corrosion problem for austenitic stainless steels, for example, is different from that of other alloys. Freedom from cracking can be achieved by impressing an electric current for cathodic protection (48). This suggests that cracking in austenitic stainless steels involves an electrochemical mechanism.

In the case of the precipitation hardenable steels, on the other hand, failure may be accelerated by making the material the cathode in an electrochemical cell (48). However, since hydrogen is discharged at the surface of the steel where the steel is the cathode, it has been suggested that this type of failure is more properly the consequence of hydrogen embrittlement.

The extensive use of steels in modern technology makes the stress-corrosion cracking of iron alloys a problem on which the attention of many investigators has been focused.

#### 2.4.3 Aluminum Alloys

Since World War II there has been an ever-increasing demand for higher performance characteristics in aircraft. High-strength aluminum alloys have been a partial answer to these demands. The development of high strength in these aluminum alloys has been accompanied by a susceptibility to stress-corrosion cracking.

Observed cracking in aluminum alloys is mostly intergranular and is caused by NaCl solutions. Most investigators agree that the stress-corrosion cracking of aluminum alloys may be the product of an electrochemical-mechanical mechanism (13, 49, 50).

#### 2.4.4 Titanium Alloys

Titanium alloys are susceptible to stress-corrosion cracking in red, fuming nitric acid, hot chloride salts, and sea water at room temperature (51, 52).

Cracking in titanium alloys appears to be primarily intergranular. Beck (51) suggests that in the stress-corrosion cracking of titanium alloys, electrochemical and surface-energy reduction mechanisms may be operative.

### 2.5 General Approach to the Stress-Corrosion Cracking Problem by Other Researchers

All alloy metals are susceptible to stress-corrosion cracking in varying degrees (53). This susceptibility is more evident in the higher strength materials, particularly those with high strength-to-weight ratios. Stress-corrosion cracking appears to be dependent not only on stress levels and environment but also on processing techniques.

The chief approach to the stress-corrosion cracking problem is that of observing the effects of metallurgical variables on the stress-corrosion cracking behavior of a particular alloy. These metallurgical variables include processing techniques, alloying elements, heat treatments, electric potentials, protective coatings, cold work, and residual stresses.

To observe the effects of all the variables named above on the stress-corrosion cracking of alloy systems, researchers have devised all sorts of testing gadgets and procedures. Practically every new paper in the field proposes a novel method for testing stress-corrosion cracking. An interesting compendium of apparatus and procedures for stress-corrosion cracking testing is offered by Humphries (54).

### 2.6 Summary

Ultra-pure metals are seldom used in their elemental form. Their characteristics are usually improved by alloying, although sometimes the price that must be paid is susceptibility to stress-corrosion cracking. Stress-corrosion cracking is a complex problem

which has been responsible for the catastrophic failure of many structures. Efforts are constantly being made to solve the problem through a better understanding of stress-corrosion cracking behavior.

## CHAPTER III

### FRACTURE

#### 3.1 Introduction

Fracture is the separation, or fragmentation, of a solid body into two or more parts under the action of stress (27). The process of fracture is considered to take place in two major steps: crack initiation and crack propagation. The second step has been further subdivided into slow crack growth and rapid, unstable fracture (34).

Fractures have been classified into two general categories: ductile fractures and brittle fractures. A ductile fracture is characterized by appreciable plastic deformation prior to and during the propagation of the crack.

Brittle fracture in metals is characterized by a rapid rate of crack propagation, with no gross deformation and very little micro-deformation. The tendency for brittle fracture is increased with decreasing temperature, increasing strain rate, and triaxial stress conditions which are usually the result of a notch.

In addition to ductile and brittle fractures, fractures in metals can be further classified into transgranular or intergranular, depending on the paths followed by the majority of the cracks. Intergranular cracking is associated with grain boundary failure while transgranular cracking follows other paths through the grain. A discussion of the major classifications of fracture follows below.

### 3.2 Brittle Fracture

Griffith's original ideas on brittle fracture, though not entirely applicable to metals (27, 55), have influenced the development of modern theories of fracture in metals. Griffith proposed that a brittle material (one which fractures in a brittle manner) contains a network of fine cracks which produce local stress concentrations of sufficient magnitude that the cohesive strength is reached at nominal stresses which are well below the theoretical value. These stresses cause the cracks to extend.

Griffith considered that in the extension of a crack in a brittle material there exists a balance between two factors: the surface energy of the spreading crack and the release of the strain energy of the applied stress fields (55). A brittle material, as opposed to a ductile material, is one which at room temperature and in a simple tensile test fractures in a brittle manner without appreciable plastic flow. Griffith established the following criterion for the propagation of a crack: "A crack will propagate when the decrease in elastic strain energy is at least equal to the energy required to create the new crack surface." (2).

Modern theories of fracture in metals are the result of extensions and modifications of Griffith's original theory. The concept of the energy balance has been retained, but other factors have been included as their importance became apparent.

A current theory of brittle fracture contends that there are four energy terms which control the growth of a crack. These four terms are:

- a. The surface energy of the crack, proportional to its length  $\ell$ ,

$$+ A\ell;$$

- b. The reduction in energy of the applied stress field proportional to the square of the applied stress and the square of the crack length,

$$- B\sigma^2 \ell^2;$$

- c. The complex plastic deformation factor that depends upon the crack length, the applied stress, and the yield point of the material,

$$+ Cf(\ell, \sigma, y);$$

- d. The energy provided by the local stress concentration at which fracture begins which is generally assumed to be proportional to  $-\log \ell$ ,

$$- D \log \ell.$$

A, B, C, and D are constants of proportionality, and the signs indicate the nature of the contribution of each term, i.e., is crack growth enhanced or hindered?

The change in energy due to the extension of the crack is

$$\Delta E = \Delta[A\ell] - \Delta[B\sigma^2 \ell^2] + \Delta[Cf(\ell, \sigma, y)] - \Delta[D \log \ell],$$

and the condition for the crack to extend or increase in length is that

$$(\partial E)/(\partial \lambda) < 0.$$

It is often suggested that in the case of metals the surface energy will be negligible compared with the plastic deformation term (27). This may be particularly true when gross deformation occurs. However, in the nucleation stages of microcracks, the surface energy term is large compared with the elastic energy (55). If the crack is to extend at all, very little of the energy available is dissipated in plastic deformation. This is the reason why cracks propagate only through brittle materials.

Once a crack forms, plastic deformation provides a means of using up the strain energy released as the crack extends (56). Thus, a plastic energy term was added to the energy balance. The plastic deformation energy term represents the energy consumed by the plastic deformation that occurs in the highly stressed region in front of the growing crack.

It should be noted that with normally accepted surface energy values (27), the cracks required to produce fracture at normal loads are much too large to be present initially in the unstressed material (55). Since it is generally supposed that fracture begins at a point of local stress concentration such as might be the result of a pile-up of dislocations (27, 28, 29, 30), the local strain energy associated with the stress concentration was also added to the energy balance.

The energy balance of the modified Griffith criterion for brittle fracture appears to be satisfactory in the light of present-day

brittle fracture mechanics (55), and experimental evidence seems to favor the dislocation mechanism of crack nucleation (34, 55).

The process of brittle fracture has been separated into three stages (34): crack nucleation, slow crack growth, and rapid fracture. A short discussion of these will be given below.

### 3.2.1 Crack Nucleation and Propagation

A. Crack Nucleation. In materials which are free of flaws, the first stage in the process of fracture is the nucleation of a microcrack or void. These defects are formed by the piling-up and coalescence of dislocation groups in the vicinity of grain boundaries or hard particles such as inclusions (11, 27, 57, 58). Figure 2 shows a series of schematic diagrams which describe the mechanisms of microcrack nucleation as a result of dislocation interactions.

As the applied stress in a tensile test increases, increasing numbers of microcracks and voids are formed (57). These act as stress concentrators and cause the material between them to fail in shear at low nominal stresses (59). Eventually, a sufficient number of voids and/or microcracks form and coalesce which leads to the development of a macrocrack (more than one grain diameter in length).

B. Slow Crack Growth. Crack growth initially occurs discontinuously (12, 24, 59). Increasing numbers of voids form ahead of the tip of the crack and join it (coalesce). Crack propagation occurs by short, rapid advances followed by waiting periods in which plastic strain ahead of the crack builds up sufficiently to cause additional

void formation and local instability. The voids formed at the tip of an extending crack are termed "precursor cracks" and have been observed using field-emission microscopy by Hoenig and Creighton (4, 5).

C. Rapid Fracture. As the crack grows longer, its ability to concentrate stress at its tip increases. Eventually, the crack is long enough to satisfy the criterion for unstable fracture and propagates rapidly causing the structure to fail. The criterion (34) for this to occur is that the applied stress reaches a value  $\sigma$  given by

$$\sigma = (2\gamma_m)/(nb)$$

where  $n$  is the number of dislocations in the pile-up having Burgers vector  $\underline{b}$  which cause microcrack and void formation and  $\gamma_m$  is the work done in microcrack propagation.  $\gamma_m$  is directly proportional to the surface energy  $\gamma_s$ .

### 3.3 Ductile Fracture

Ductile fracture appears to have been studied much less extensively than brittle fracture, owing perhaps to the fact that it is a much less serious problem in engineering structures. Ductile fracture is described as occurring with appreciable gross plastic deformation and by a slow tearing of the metal with the expenditure of considerable energy (27).

Ductile fracture, in a tensile test, is usually preceded by a localized reduction in diameter called necking. Necking begins at the point of plastic instability where the increase in strength due to strain hardening fails to compensate for the decrease in

cross-sectional area. This occurs at maximum load or at a true strain equal to the strain-hardening coefficient (27).

In ductile fracture, fine cavities form in the necked region. Under continued strain these cavities grow and coalesce into a central crack. This crack grows in a direction perpendicular to the axis of the specimen until it approaches the surface. It then propagates along localized shear planes at roughly  $45^\circ$  to the axis of the specimen to form the "cone" part of the "cup and cone" type of fracture exhibited by many metals and alloys of technical importance.

The previous discussion of both brittle and ductile fracture has ignored the possible effect of a chemically active or corrosive environment. The following section will touch on crack nucleation and cracking susceptibility in stress-corrosion cracking.

#### 3.4 Cracking Susceptibility in Stress-Corrosion Cracking

The stress dependence of stress-corrosion cracking suggests that a dislocation pile-up mechanism may be responsible for crack nucleation. The dislocation mechanism coupled to the enhanced corrosive action of the environment may then be responsible for the catastrophic results observed in stress-corrosion cracking described in Section 2.1.

Uhlig's (60) position on cracking susceptibility is that the pile-up of dislocations is certainly a feature of stress-corrosion cracking susceptibility. He states, however, that dislocations alone cannot be responsible for profuse cracking and that there must be some element which segregates and coalesces at the dislocations. This element, which can be in the form of an alloying component, or in the

form of impurities, in combination with the pile-up of dislocations and the corrosive environment may cause stress-corrosion cracking susceptibility.

There is no indication in the literature as to the exact role of the element proposed by Uhlig (60) in causing stress-corrosion cracking susceptibility. That is to say, it is very difficult to pinpoint whether the additional element mentioned by Uhlig (60) is responsible for the establishment of anodic paths or whether it alters the oxidation or corrosion properties of the parent metal. It is quite possible that in some alloys the former is true, while in others the latter may be true; and yet, in other alloys, the element proposed by Uhlig (60) may be responsible for both establishing anodic paths and altering the corrosion properties of the parent metal. Additional research is essential in this area.

In the absence of data on the exact role played by the critical element discussed above, many researchers have found it less difficult to postulate stress-corrosion cracking susceptibility criteria in terms of the role played by dislocations.

Thomas and Allio (26) contend that their observations show that if dislocations become piled-up on slip planes due to a low stacking fault energy (see Appendix A for a short treatment of stacking fault energy), a susceptible alloy results. On the other hand, if a cellular arrangement is obtained as a result of high stacking fault energy, the alloy is not susceptible to stress-corrosion cracking. This may be due to the fact that if the dislocations are distributed in a cellular

arrangement, crack nucleation, according to the mechanisms described in Fig. 2, is virtually impossible; and, thus, stress-corrosion cracking is either nonexistent or considerably retarded.

Swann (46) states that the distribution of dislocations is dependent upon the stacking fault energy of the material. Pure face-centered cubic (fcc) and body-centered cubic metals (bcc) usually have relatively high stacking fault energies (61), although alloying additions and impurities tend to lower the energies (46, 61). In metals having low stacking fault energies cross slip of dislocations becomes more difficult than in metals with a high stacking fault energy. This is because the region of stacking fault is more extensive in metals of low stacking fault energy, and the partial dislocations (a lower energy configuration for unit dislocations, see Appendix A) which bound the faulted region must be constricted before cross slip can occur.

When cross slip becomes difficult, dislocations are forced to move on parallel planes tending to produce coplanar arrays; this condition produces a susceptible alloy (26). In the high stacking fault energy metals, on the other hand, cross slip may occur more easily, and tangles of dislocations may be formed which result in a non-susceptible alloy (26). In the stress-corrosion cracking of copper-zinc alloys in ammonia, for example, Thompson (62) has measured the stress-corrosion cracking susceptibility as a function of composition. His data, in terms of the time (in hours) required to cause 50 percent relaxation in U-bend specimens indicate that susceptibility to stress-corrosion cracking increases with zinc content. The times for 50 percent

relaxation in 85-15 red brass, 70-30 brass, and 60-40 Muntz metal are 1.53, 0.44, and 0.35 hours, respectively. Stacking fault energies for these alloys are 30, 13.3, and 7 ergs/cm<sup>2</sup>, respectively (63). It can thus be seen that the stacking fault energy and the dislocation distribution may be directly related to the stress-corrosion cracking susceptibility of alloys.

Although many researchers (46, 60, 61, 64) favor the idea that coplanar arrays of dislocations may be partly responsible for stress-corrosion cracking susceptibility, further studies in this area are necessary in order to produce more quantitative data to support this view.

### 3.5 Intergranular and Transgranular Cracking

Fracture, whether due to stress-corrosion cracking or to simple stress alone, can be either intergranular or transgranular. There is, however, a fundamental difference between "normal" cracking (i.e., cracking in the absence of stress-corrosion cracking) and stress-corrosion cracking. In the normal cracking of metals, the effects of corrosion, if any, are neglected as having little or no bearing on the fracture process. In the absence of a corrosive atmosphere, intergranular and transgranular cracking seem to depend on whether the metal fails in a brittle or ductile manner in a simple tension test. Ductile metals, which fail after gross plastic flow, usually fracture transgranularly when pulled to destruction, in simple tension test, in the absence of corrosion (11). On the other hand, brittle metals, which

fail with appreciable plastic deformation, usually fracture intergranularly when pulled to destruction in a simple tension test (11).

In stress-corrosion cracking it is often found that intergranular cracking shows some dependence upon heat treatments of the type which produces a grain boundary precipitate. Intergranular cracking is further associated with a susceptibility to selective corrosion along more or less continuous paths (grain boundaries) which are anodic, in a specific corrosive medium, to the areas comprising the major part of the structure. Transgranular cracking, on the other hand, appears to be less sensitive to the earlier heat treatment of the alloy.

It was suggested in Section 2.1 that the two modes of cracking stand at opposite ends of a spectrum and that a transition may occur from one mode to the other as the alloy composition is changed or the ambient conditions are altered. Such a transition has been shown to occur in some copper alloys by varying the degree of deformation prior to the stress-corrosion cracking test (11). Similarly, Mattson (65) has reported a transition in the mode of cracking observed in alpha-brass as the pH of the environment was varied.

These observations suggest that a rigid division between transgranular and intergranular cracking is undesirable in stress-corrosion cracking studies. This suggestion notwithstanding, it appears that, in stress-corrosion cracking, intergranular and transgranular cracking differ in that, in intergranular cracking, fracture is thought to occur by corrosion with stress assisting in the process of cleavage; in transgranular cracking, on the other hand, fracture is thought to occur by mechanical failure with corrosion assisting in the process.

In the following chapters it will be shown that the stress-corrosion cracking characteristics of U-10<sup>w</sup>o Mo are dependent upon heat treatments and changes in the environment. The next chapter will treat the stress-corrosion cracking of uranium-molybdenum alloys.

## CHAPTER IV

### STRESS-CORROSION CRACKING IN URANIUM-MOLYBDENUM ALLOYS

#### 4.1 Introductory Remarks

Dilute uranium-molybdenum alloys are being used as fuel and structural materials in certain types of reactors (1, 2). These alloys have been found to be susceptible to stress-corrosion cracking in atmospheric air (3). Susceptibility to stress-corrosion cracking is reported in the literature in terms of time for a specimen to fail, or time for the first visible cracks to appear under given conditions of alloy composition, environment, heat treatment, loads, and other metallurgical variables (62, 66).

#### 4.2 Work by Other Researchers

The susceptibility to stress-corrosion cracking of U-10 <sup>w</sup>/<sub>o</sub> Mo in laboratory tests has been found to be dependent upon the processing, and heat treatment, grain size, and the impurity content of the metal, and the strain rate in a simple tension test.

The processing of the alloy and the heat treatments determine to a certain extent the susceptibility of the alloy. It has been shown (67) that if the alloy is water quenched, after being rolled at 950°C and annealed at 825°C, it has a greater susceptibility to stress-corrosion cracking than if it is furnace cooled. Furthermore, if a specimen is vacuum cast, and then stressed in vacuum, it will sustain stresses which

would otherwise result in early failure had it been loaded in atmospheric air (67). It also appears (67) that holding a specimen under stress for long periods of time in a vacuum will prevent cracking or will slow down the cracking rate when air is again introduced.

Very little work has been done on the effect of grain size on the stress-corrosion cracking behavior of U-10 <sup>w</sup>/o Mo. Peterson et al. (66) believe that grain size has no appreciable effect on the fracture process and that, therefore, it is not a controlling parameter in the stress-corrosion cracking of this alloy.

Impurities, on the other hand, appear to have a direct influence on the stress-corrosion cracking behavior of U-10 <sup>w</sup>/o Mo. Peterson et al. (66) have found that alloys containing an increased amount of carbon (up to 400 ppm) are more susceptible to stress-corrosion cracking than those with less carbon (64 ppm). The effect of impurities other than carbon has not been investigated.

The strain rate at which tensile tests on U-10 <sup>w</sup>/o Mo have been performed seems to have a bearing on the stress-corrosion cracking behavior of this alloy. Tensile tests have been performed (66, 77) at different cross-head (pulling) speeds. Maximum ductility has been obtained at cross-head speeds of 0.05 in./in./min. At lower cross-head speeds, U-10 <sup>w</sup>/o Mo exhibits profuse surface cracking which becomes progressively more severe as the strain rate is decreased. At higher cross-head speeds, a loss in ductility has been observed; however no surface cracks or oxide film were apparent.

The behavior of U-10 <sup>w</sup>/o Mo at lower cross-head speeds may be due to the fact that at lower strain rates (below 0.05 in./in./min.),

the corroding agent has more time to react with any given surface imperfection. This would lead to greater surface damage. At higher strain rates, on the other hand, the corrosion film breaks off as it is formed and constantly exposes fresh material to the environment. The decrease in ductility may be ascribed to a work hardening phenomenon and is to be expected at higher strain rates. Failure of the tensile specimens at higher strain rates may begin from within the specimen, as is the case of some steels, which would explain the absence of surface cracking phenomena.

Most investigators have implicitly subdivided the problem of stress-corrosion cracking into three parts: (1) determination of the mode of cracking, (2) determination of the agent or agents responsible, and (3) investigation of possible protection techniques. Each of these will be discussed below.

#### 4.2.1 Mode of Cracking

The mode of cracking of U-10 <sup>w</sup>/<sub>o</sub> Mo in atmospheric air appears to be a mixture of intergranular and transgranular cracking, with no preponderance of any one mode. Greenspan's statement (68) summarizes the general concensus on this subject. He states that his observations "... thus far, give no clear indication of whether cracking is intercrystalline or transcrystalline." The question of whether cracking is predominantly intergranular or transgranular in a particular environment must be resolved.

In the investigation of fracture modes, a critical stress (stress below which cracking is not observed under the usual stress-

corrosion cracking conditions) has been sought. Peterson and Vandervoort (66) report this stress to be 37,000 psi for U-10 <sup>w</sup>/<sub>o</sub> Mo. However, this value should not be relied upon for design purposes.

#### 4.2.2 Agent or Agents Responsible for Stress-Corrosion Cracking

Peterson and Vandervoort (66) conducted tests to determine which of the components of atmospheric air are responsible for the stress-corrosion cracking behavior of the alloy. They performed these tests by loading the specimens in a test chamber evacuated to about  $10^{-5}$  torr and then back-filling the chamber with one specific gas at a time. They concluded that "dry" oxygen was responsible for stress-corrosion cracking and that the oxide layer formed on U-10 <sup>w</sup>/<sub>o</sub> Mo is non-protective. They did not, however, indicate how dry the oxygen was, nor did they indicate what effect different concentrations of gases might have on the overall stress-corrosion cracking behavior of the alloy. They recommended further studies of the effect of water vapor on the ductility of the alloy.

#### 4.2.3 Possible Protection Techniques

Many attempts have been made to improve the general stress-corrosion cracking behavior of U-10 <sup>w</sup>/<sub>o</sub> Mo. Where use of metals in corrosive media is intended the most common corrosion preventives are coating or plating, and further alloying. Attempts at nickel plating have been made on U-10 <sup>w</sup>/<sub>o</sub> Mo, but these have been fruitless (69). The two main drawbacks are breaking of the nickel coating, which exposes the alloy to atmospheric air, and hydrogen absorption during the

coating process. Hydrogen embrittlement was discussed in Section 2.3, and seems to be a severe problem with U-10 <sup>W</sup>/<sub>b</sub> Mo.

A coating technique which does not involve hydrogen evolution is vapor deposition in a vacuum system. U-10 <sup>W</sup>/<sub>b</sub> Mo can be coated in this manner with a layer of aluminum. The specimen is subsequently heat treated to convert the deposited coating into  $UAl_3$ . Vapor deposition seems to work well on many alloys. However, a recent failure of an aluminum-coated U-10 <sup>W</sup>/<sub>b</sub> Mo bolt in Oak Ridge (70) has cast some doubts as to the effectiveness of this coating on uranium-molybdenum alloys.

There is a difference of opinion as to the effect of further alloying U-10 <sup>W</sup>/<sub>b</sub> Mo with titanium and/or niobium. Peterson et al. (66) report that niobium addition does not decrease the cracking susceptibility, but that a 1 <sup>W</sup>/<sub>b</sub> titanium addition results in a critical stress (stress below which cracking is not observed under the usual stress-corrosion cracking conditions) of 108,000 psi which is the highest yet reported for uranium alloys. Greenspan (68), on the other hand, reports that uranium-molybdenum alloys with titanium exhibited delayed fracture (stress-corrosion cracking) and failed at lower values of strain, compared with U-10 <sup>W</sup>/<sub>b</sub> Mo. At present, the entire question must be considered as unresolved.

A well-known corrosion protection technique used with many alloy systems is that of cathodic protection using a sacrificial anode. Many steels can be cathodically protected (44) and the stress-corrosion cracking of alpha-brass can be influenced by using electric DC fields (71). There are no indications in the literature that these techniques have been investigated for uranium alloys.

### 4.3 General Characteristics of Uranium-Molybdenum Alloys for Reactor Applications

The stress-corrosion cracking behavior of any susceptible alloy is influenced by many of its physical properties and characteristics. Unfortunately, the effect of only a few of these properties on stress-corrosion cracking has been investigated in any one alloy system.

The crystal structure and the phases of an alloy whether actually present or potential (resulting from the decomposition of a metastable phase) influence its stress-corrosion cracking behavior. A metastable phase may decompose, or it may precipitate and coalesce (14) in such a way that potential anodic paths are formed (15, 16, 17). These paths are sites for selective dissolution and enhanced corrosion. The next section discusses the phases encountered in uranium alloys.

#### 4.3.1 Phases Encountered in Uranium Alloys

Uranium is trimorphic (72). The three distinct phases are labelled  $\alpha$ ,  $\beta$ , and  $\gamma$  respectively. The alpha form normally exists at temperatures below 662°C and exhibits an orthorhombic crystal structure. The beta form is usually limited to the temperature range 662 to 770°C. This phase is complex tetragonal. The gamma form is body-centered cubic and persists above 770°C to the melting point at 1130°C.

The gamma phase, though metastable at room temperature, is by far the most important. When this phase is retained at room temperature through alloying and heat treatments, (2, 73, 74) the material that results possesses highly desirable physical properties. A gamma-stabilized uranium alloy (homogenized in the gamma region, followed by

a low temperature quench), being body-centered cubic, possesses a high degree of isotropy and ductility, and displays very good thermal stability when compared with other uranium alloys. Molybdenum and vanadium are two elements which produce expanded gamma-phase regions. The terminal solubilities of these elements with uranium are 43 percent for molybdenum and 12 percent for vanadium (72).

In addition to the phases discussed above, several other phases influence the corrosion behavior of uranium alloys. In general, these phases are obtained by specific heat treatments (72). Upon heating to subcritical temperatures (below 662°C), the metastable gamma phase transforms into alpha plus a second phase, the structure of which depends upon the alloying elements involved. Specifically, this second phase is the ordered tetragonal, epsilon phase in the uranium-molybdenum system. The alpha and epsilon phases are coherent and tend to precipitate through a nucleation and growth process. The precipitation renders these alloys precipitation hardenable.

Coherent precipitates usually hinder dislocation motion and increase the strength of the alloy. The precipitates may, however, affect corrosion behavior if they coalesce, as discussed above. Therefore, a very close control in heat treating is essential because, while precipitation may be beneficial, coalescence may be undesirable.

In the discussion of composition, phases, and heat treatment of an alloy system it is always useful to refer to the equilibrium diagram and the TTT curves of the alloy. The equilibrium diagram of the U-Mo system (73) is shown on Fig. 3a and the TTT curves for an U-6<sup>a</sup>% Mo

(2.5 <sup>w</sup>%) alloy (74) are shown on Fig. 3b. The value of these figures to the metallurgist for processing and heat treating of alloys is self-evident. Due to the gamma-retaining tendency with increasing molybdenum, it is expected that a 10 <sup>w</sup>% Mo (for which no TTT curves are available yet) should exhibit a TTT curve displaced to the right. This provides more time in heat treatments to retain the  $\gamma$  phase. Therefore, Fig. 3 will be used throughout this work as a conservative estimate for the heat treatment of a 10 <sup>w</sup>% Mo alloy.

#### 4.3.2 General Characteristics of U-10 <sup>w</sup>% Mo for Reactor Applications

The characteristics of U-10 <sup>w</sup>% Mo for reactor applications have been summarized by Rienecker and Moran (2) and Hoge (75) in the following manner:

- a. Strength: The yield strength of the fully annealed alloy is 130,000 psi when tested in simple tension in a vacuum. Dynamic loading increases the tensile strength and lowers the ductility.
- b. Dimensional stability: U-10 <sup>w</sup>% Mo is not subject to ratcheting during thermal cycling. It has a very isotropic coefficient of linear expansion.
- c. Gamma stability: All gamma-stabilized uranium alloys are metastable at room temperature and subject to transformation when heated to approximately 300°C. U-10 <sup>w</sup>% Mo, however, is the most stable uranium alloy presently known, and is entirely satisfactory from this standpoint.

d. Homogeneity: U-10 <sup>w</sup>/o Mo is not subject to gross segregation. The microsegregation which does occur can be relieved readily by a short homogenization treatment.

e. Impurities: Carbon content should be kept low, below 200 ppm. High carbon content tends to reduce both ductility and tensile strength.

f. Reservations: U-10 <sup>w</sup>/o Mo is subject to stress-corrosion cracking in the presence of oxygen. The alloy should be protected from the atmosphere, particularly if high residual stresses are present.

#### 4.4 Summary

It seems to be well established that uranium-molybdenum alloys are susceptible to stress-corrosion cracking. It also appears that this susceptibility depends on the method of processing, the impurity content, and the strain rate, and that atmospheric oxygen is partly responsible for stress-corrosion cracking.

Chapter V will discuss the research effort at the University of Arizona.

## CHAPTER V

### RESEARCH EFFORT AT THE UNIVERSITY OF ARIZONA

#### 5.1 Initial Considerations

The specific research at the University of Arizona was aimed at determining the following:

- a. The mode of cracking in the stress-corrosion cracking of U-10<sup>w</sup>/o Mo;
- b. The agent or agents responsible for the stress-corrosion cracking of U-10<sup>w</sup>/o Mo;
- c. The possibility of developing protective techniques against the stress-corrosion cracking of U-10<sup>w</sup>/o Mo which had not been tried by other researchers, namely, cathodic protection, application of static DC fields, and gas shielding.

The stress-corrosion cracking behavior of a susceptible alloy is normally investigated by studying the mode of cracking and the specific effects of the particular ambient atmospheres that promote cracking. Closely coupled to any stress-corrosion cracking research effort, there is usually an investigation of possible protective techniques.

It is important to understand the mode of cracking, in the early stages of fracture in order to determine the possible mechanisms of

cracking. A definite answer should be given to the question of whether cracking is due to mechanical failure assisted by corrosion or whether it is primarily due to corrosion which is assisted by the residual or the applied stresses.

Directly related to establishing the mode of cracking is, of course, determining the particular environment which promotes cracking. Specifically, in the U-Mo system, it is of great importance to determine which of the components of atmospheric air are responsible for stress-corrosion cracking and to what extent.

Any protective technique would be of great importance. Typical protection methods might include cathodic protection (used on steel and brass), coatings of various types to retard corrosion, and selected heat treatments to reduce stress-corrosion cracking sensitivity.

A protective atmosphere might also be used since the operation of the Aberdeen Fast-Burst Reactor subjects most of its structural members to tensile stresses of short (15 minutes) duration (70). If during the cyclic operation of the reactor its structural members were "bathed" with an inert atmosphere (in this case, a gas believed not to cause stress-corrosion cracking), the probability of stress-corrosion cracking might be decreased. Special cyclic-loading tests with protective "gas shields" have not been tried before, and the possibility of such a simple protective technique warrants investigation.

These topics, with the exception of coatings, were considered the most significant and were chosen for investigation at the University of Arizona.

## 5.2 Experimental Apparatus and Techniques

### 5.2.1 Apparatus

A. The Field-Emission Microscope. The determination of the mode of cracking required a means of detecting fracture in its initial stages. A field-emission microscope of cylindrical geometry has been found useful in studies of the early detection of brittle fracture (4, 5). The field-emission microscope of cylindrical geometry, to be discussed below (see Fig. 4), was ideally suited for this investigation for not only did it permit the early detection of microcracks but also provided a vacuum chamber for conducting tensile tests in desired atmospheres.

The field-emission microscope, used by Hoenig and Creighton (4, 5) and used in this investigation, is shown in Fig. 4. The pulling assembly and base plate were modified in this investigation to permit the introduction of any desired gas or combination of gases into the test chamber (see below).

The field-emission microscope has a high magnification and resolution and is almost uniquely suited for observations of microcracks. Since the field-emission microscope is relatively new as a metallurgical instrument, a short description will be given here.

Normally, metals at room temperature do not emit electrons, however, in the presence of a strong electric field gradient, electrons can tunnel out through the reduced potential barrier. Since this tunneling is a function of the local field gradient and the local work

function, the emitted electrons can be used to produce a highly magnified image of the surface by allowing them to strike a phosphor screen. Because the electron emission is dependent upon the local field gradient, smooth surfaces emit few electrons except at very high fields. On the other hand, cracks, extrusions, or other surface defects, having sharp edges, emit strongly since the field gradient is very high in the vicinity of these defects. This indicates that the field-emission microscope should be most useful for detection of microcracks on otherwise smooth surfaces.

Normally, a cylindrical field-emission microscope geometry produces magnification only in the radial direction because a smooth wire at the center of a cylinder produces a purely radial electrical field. However, if there is a break in the smooth surface of the inner cylinder, the field near the break becomes three dimensional and the area of the break is highly magnified. The reason for this is clear if it is recalled that the field gradient depends on the relative radii of the inner and outer cylinders; if a crack forms, the edge radii are of atomic dimensions and a very high field gradient is formed near these crack edges.

Since the electrons receive most of their acceleration near the crack edge and are always traveling perpendicular to the field lines, they tend to spread out and produce the magnified image observed in the cylindrical field-emission microscope.

The cylindrical field-emission microscope, which was modified for use in this investigation, shown in Fig. 4, consisted of a vacuum

system, a phosphor-coated glass pipe (76), and a wire-pulling assembly. Two pin vises (L. S. Starrett Company, Athol, Mass.) held the wire specimen. The bellows was made from electro-deposited nickel (Servometer Corporation, Clifton, N. J.) and allowed linear movement of the assembly within the vacuum chamber. The motor was a 5-RPM AC motor (Carter Motor Co., Chicago, Illinois) which, coupled through a 20:1 reduction gear, was capable of pulling on the assembly at any desired rate of strain. The vacuum system was capable of pressures in the range of  $10^{-7}$  torr. The pressure was measured on an ETI, Alpert-type ion gauge No. ETI-4336TP (Electron Technology Inc., Kearny, N. J.) in conjunction with a Veeco vacuum gauge control panel type RG (Vacuum-Electronics Corp., Plainview, L. I., N. Y.) backed by a Welch No. 1397B mechanical pump (W. M. Welch Scientific Company, Chicago, Illinois). Backing pressures were measured on a Pirani gauge type GP-145 (CVC, Rochester, N. Y.).

The modified pulling assembly which was used throughout this investigation is shown on Fig. 5a. In addition to the equipment described above, the modified assembly included a cantilever beam load cell (courtesy of the Instron Corporation, Long Beach, Calif.), provisions for AC heating of the specimen, and a feedthrough for admitting the gases into the field-emission microscope chamber.

The load cell contained two Pixie solid state strain transducers (courtesy of the Endevco Corporation, Pasadena, Calif.). The output signal of the strain transducers was fed directly to a Rustrak recorder model 88 (Rustrak Instrument Co., Inc., Manchester, N. H.) without any additional amplification.

The high voltage which extracts the electrons from the specimen and accelerates them toward the field-emission microscope screen was supplied by a Spellman model PN-30, 0-30KV DC high-voltage power supply (Spellman High Voltage Co., Bronx, N. Y.).

B. Gas Mixing and Washing Equipment. The gases used in this investigation were for the most part dry, "extra dry grade" (- 70°F dew point) (Matheson Company, Newark, Calif.), and were admitted into the field-emission microscope chamber directly from the cylinder through a micrometer valve. However, when mixtures of gases were desired or when the effect of water vapor content was desired, the gases were passed through the gas mixing chamber, Fig. 5b, and gas washer tank, Fig. 5c.

The gas mixing chamber consisted of three gas inlets and a series of cross-connected baffles to insure mixing. The gas washer tank contained a special well for a heater. The heater was used for raising the temperature of the water to increase the water vapor content of the gas being washed.

C. Apparatus for Heat Treatment. Heat treatments were carried out in a special vacuum furnace (77). One end of an Inconel-600 tube was enclosed in a high-temperature oven (Blue M Electric Company, Blue Island, Illinois). The other end was kept at approximately 20°C by means of a cooling coil filled with circulating chilled water. This particular arrangement permitted the instantaneous quenching of thin-wire specimens by pulling the refractory boat, which held the specimens, from the high-temperature region to the low-temperature region. This

was accomplished by means of a chain attached to the boat on one end and to a magnetic feedthrough on the other. Turning the magnetic crank pulled the boat into the low-temperature zone.

D. Apparatus for Cathodic Protection and Electric Fields.

Cathodic protection experiments were conducted using the apparatus and electrical setup shown on Fig. 6. The specimens and sacrificial anodes were fed through the rubber stopper into the container as shown. The gas ports permitted the circulation of any desired gas through the container. Impressed voltages were supplied by a Heath model EUW-15 University Power Supply (Heath Company, Benton Harbor, Mich.).

The effect of static electric DC fields on the stress-corrosion cracking behavior of U-10<sup>w</sup>/o Mo was studied using the apparatus and electrical circuit shown on Fig. 7. The apparatus consisted of a glass envelope which contained the specimen and a cylindrical, stainless steel collector. The gas ports permitted the circulation of a slow-flowing gas within the container, and the grounding shields prevented any leakage currents between specimen and collector.

Impressed DC voltages were supplied by a Heath model EUW-15 Universal Power Supply (Heath Company, Benton Harbor, Mich.), and the micro-ammeter was a Hewlett-Packard model 425-A (Hewlett-Packard Co., Palo Alto, Calif.).

E. Apparatus for Cyclic Loading of U-10<sup>w</sup>/o Mo Specimens. The apparatus used in the cyclic-loading tests is shown in Fig. 8. The two pin vices held the wire specimen. One pin vise was stationary while the other one was attached to the follower of an eccentric cam which

caused back-and-forth motion in the horizontal plane. Motion of the cam through the crank loaded and unloaded the specimen. The crank was actuated manually.

Directly below the specimen was a gas diffuser in the form of a half cylinder which ran along the length of the specimen. Four small tubes from a common manifold exhausted a desired gas (in this case, an inert gas, believed not to cause stress-corrosion cracking) through the diffuser. To insure complete envelopment of the specimen by the gas, the diffuser was filled with glass wool. The glass wool kept gusts of ambient air from penetrating the "protective" gas shield.

An optical microscope could be mounted directly above the specimen. Observations of the specimen could thus be made while the test was in progress by lifting up the glass wool.

F. Miscellaneous. Test specimens were electropolished using two Heath-kit model IP12 battery eliminators in series (Heath Company, Benton Harbor, Mich.). The cathode was a U-10<sup>w</sup>o Mo specimen, and the electrolytic bath was contained in a Teflon tray (Van Waters and Rogers, Inc., San Francisco, Calif.).

Optical examination of the specimens was done on a Unitron series MEC inverted metallurgical microscope (Unitron Instrument Co., Newton Highlands, Mass.) equipped for polarized light microscopy and capable of magnifications of up to 1200X.

Photomicrographs were taken using both high-speed Kodak 35mm film and Polaroid film.

The experimental techniques are discussed below.

### 5.2.2 Experimental Techniques

A. Specimen Preparation. The U-10<sup>W</sup>/<sub>o</sub> specimens used throughout this investigation were in the form of thin wire (0.01 in. and 0.02 in. in diameter). The specimens were supplied by the U. S. Army through Oak Ridge National Laboratory (ORNL), Union Carbide Corporation, Nuclear Division, Plant Y-12, Oak Ridge, Tennessee. The specimens were prepared from U-10<sup>W</sup>/<sub>o</sub> Mo rod stock by swaging down to within a few mils of the final diameter and then were cold drawn to final dimensions (78).

In this investigation, some of the specimens were used "as-received" (cold drawn), and other were heat treated; see Section 1 below. All of the specimens were electropolished; see Section 2.

1. Heat Treatment. Heat treatment of the U-10<sup>W</sup>/<sub>o</sub> Mo specimens was aimed at changing several undesirable properties of the "as-received" stock, namely, high residual stresses; large, elongated grains; and extremely brittle behavior. These characteristics were disclosed in a preliminary examination of the "as-received" specimens. The preliminary examination consisted of a metallographic examination and a simple tension test.

The specimens to be heat treated were cut into 5-in. lengths and were cleaned by swabbing with acetone. This removed most of the lubricant left on the surface in the final cold drawing operation. The specimens were fitted into a ceramic, circular tube and placed on a refractory boat. The cylindrical tube was tight fitting and insured that

the specimens remained straight during heat treatment. The refractory boat was introduced into the vacuum furnace (77) and positioned at the forward (high-temperature) end. The vacuum furnace was placed in the high-temperature oven and sealed. The vacuum system was turned on, and the temperature of the oven was raised in 50°C increments. The vacuum system of the furnace operated at  $10^{-5}$  torr during heat treatment.

The heat treatments performed on the U-10<sup>w</sup>/o Mo specimens were: a stress-relief anneal for some, gamma stabilization (gamma homogenization followed by a low-temperature quench) for others, while still others were given a tempering treatment to relieve the cooling stresses induced during the gamma-stabilization treatment.

a. Stress-Relief Anneal. The stress-relief anneal was performed at 300°C for 16 hours. The specimens were placed in the high-temperature end of the vacuum furnace and after 16 hours were allowed to cool in the furnace. This treatment improved the ductility of the specimens but retained the large, elongated grain structure.

b. Gamma Stabilization. The gamma homogenization was performed at 800°C for 24 hours. Figure 3 shows that the 800°C temperature insures a  $\gamma$  structure for 10<sup>w</sup>/o Mo alloy. After 24 hours at 800°C, the specimens were quenched

by pulling the refractory boat to the region of the vacuum furnace which was maintained at  $\approx 20^{\circ}\text{C}$ ,

The gamma-stabilization treatment resulted in a gamma structure with equiaxed grains approximately 50  $\mu$  in diameter. The gamma structure was observed in the metallograph and compared with available standards (79). Grain size was measured using the wide-field filar micrometer eyepiece of the Unitron metallurgical microscope. The gamma-stabilization treatment also resulted in residual cooling stresses induced by the low-temperature quench.

c. Tempering. In order to relieve the cooling stresses induced during the gamma-stabilization treatment, U-10<sup>W</sup>/o Mo specimens were further heat treated at 300°C for 24 hours. This tempering treatment induced some alpha precipitates (79) which fortunately do not coalesce (2, 75).

2. Electropolishing. Specimens of U-10<sup>W</sup>/o Mo were electropolished by complete immersion in the solution recommended by Woods et al. (80). The solution consisted of 5 parts ortho-phosphoric acid, 5 parts ethylene glycol, and 8 parts ethyl alcohol. Electropolishing was accomplished using uranium as the cathode, at a current density of 4.2A/in.<sup>2</sup> for 30 - 40 minutes (81).

Electropolishing of U-Mo alloys in the solution described above is accompanied by the build-up of a tarnish or film

which retards or even stops the polishing process. As the tarnish builds up, a decrease in electrolytic current is observed, and the tarnish must be removed. Removal of the film, in this investigation, was accomplished by agitating the electropolishing solution with air bubbles. Several pieces of Teflon tubing were partially immersed in the solution alongside the specimen. Laboratory air, exhausting through a manifold was allowed to bubble through these tubes into the solution at a rate which kept the tarnish build-up at a minimum. This rate was determined by the indication, in a milliammeter, of the constant electropolishing current discussed above.

Once the surface of the specimen was polished, the center portion of each specimen was again immersed in the solution for approximately 5 minutes. This produced a thinned-out region in the center of the specimen in which stress-corrosion cracking effects were intentionally concentrated during the investigation. Using this technique, only a region of approximately 0.5 in. in length needed to be closely examined for stress-corrosion cracking behavior. Final diameters in this "gage length" were approximately 0.0085 in. and 0.0175 in.

After electropolishing, the specimens were washed in distilled water and rinsed in ethyl alcohol. The specimens were subsequently dried in warm air.

B. Tests in the Field-Emission Microscope. The tests performed in the field-emission microscope can be classified into two major groups: dry tests and wet tests. The dry tests utilized gases of the "extra dry grade" (Matheson Company, Newark, Calif.), and the wet tests included the effect of water vapor content of the gas. In the dry tests, the following phenomena were investigated: the effect of heat treatment and the effect of the dry gases at various stress levels on the over-all stress-corrosion cracking behavior of U-10<sup>W</sup>/o Mo. In addition, conditions were investigated for setting a tentative "critical stress" value. In the wet tests, the combined effect of water vapor and specific gases on the stress-corrosion cracking of U-10<sup>W</sup>/o Mo was investigated.

In both dry and wet tests, tensile specimens were electropolished and then statically loaded in the field-emission microscope to predetermined stresses under the influence of a particular gas or combination of gases. At discrete intervals of time the specimens were examined in the field-emission microscope for indications of early fracture, i.e., microcracks. This was accomplished through a close observation of the strain sensing equipment for any changes in the load-holding capabilities of the specimen and by field-emission microscopy to locate any cracks on the specimen itself.

In the event that microcracks were detected, the specimens were removed from the field-emission microscope and examined with the aid of a metallurgical microscope to determine whether cracking was intergranular or transgranular. The time-consuming step of "hunting" for cracks in the metallurgical microscope was avoided by the accurate

location of the microcracks through the use of the field-emission microscope.

The specimens were reloaded in the field-emission microscope and pulled to failure at a strain rate of 0.05 in./in./min. Some of the specimens were pulled to failure in the particular atmosphere which originally caused the cracks, and others were pulled to failure in vacuum. The final fracture characteristics, i.e., fracture stress, mode of fracture, and percent reduction in area, were noted in every case.

By reloading the specimens in a particular atmosphere and pulling them to failure, it was possible to study the effect of that atmosphere on the behavior of the specimen under continuous loading. By reloading other specimens and pulling them to failure in vacuum, on the other hand, it was possible to study the extent of the permanent damage suffered by the structure of the specimen during its initial exposure to the gas.

The choice of predetermined stress levels for the static tests was aimed at trying to find a critical stress for  $U-10^{W/o}$  Mo. Test loads ranged from no load to approximately 60 percent of the yield strength of the alloy.

Special time to fail tests were performed in the field-emission microscope by loading tensile specimens to predetermined stress levels in specific atmospheres. The specimens remained statically

loaded until failure. Stress levels were in the range of 10,000 psi to 80,000 psi.

The gases used in the tests described above were oxygen, hydrogen, nitrogen, carbon dioxide, helium, argon, and water vapor. In the case of the inert gases, Gorman (82) states that they are often contaminated, especially with water vapor, at the supplier's facility. To insure the dryness of the inert gases in this investigation, they were passed through Drierite brand  $\text{CaSO}_4$  (W. A. Hammond Drierite Co., Xenia, Ohio). Argon was further purified by a heated CVC Copper Foil Glass Trap type TFG-51 (CVC, Rochester, N. Y.).

C. Cathodic Protection and Electric Fields. The investigation of the possibility of cathodic protection was conducted using specimens of U-10<sup>w/o</sup> Mo and other metals as sacrificial anodes. The tests were performed in the presence of specific ambient atmospheres while impressed DC voltages were varied in magnitude and polarity. The specimens were periodically examined, using an optical microscope for signs of stress-corrosion cracking.

The effect of static electric DC fields was studied by applying static DC fields between U-10<sup>w/o</sup> Mo wire specimens and a cylindrical, stainless steel collector. Both specimen and collector were contained within a glass envelope which permitted the circulation, within the envelope, of any desired gas. While circulating a particular gas, the impressed DC voltage was varied in magnitude and polarity. As in the previous case, the specimens were

periodically examined metallographically for the existence or absence of stress-corrosion cracking.

D. Cyclic-Loading Tests. Electropolished specimens were loaded cyclically in tension to predetermined stress amplitudes in the apparatus of Fig. 8 and at the same time bathed with gases presumed to be inert (in this case, not responsible for stress-corrosion cracking). Each specimen was loaded an average of 6 cycles per hour with each cycle corresponding to one turn of the eccentric cam shown on Fig. 8. After each cycle, the protective "gas shield" was shut off, and the specimen was kept unloaded in atmospheric air. The behavior of U-10<sup>w</sup>Mo under the conditions just described was carefully noted in terms of the number of cycles, at 36,000 psi, for the first surface microcracks to appear. This stress level was chosen on the basis of results of other experiments to be discussed in Chapter VI. The tests were performed in ambient air, dry, laboratory air (laboratory air carefully dried by passing it through Drierite brand CaSO<sub>4</sub> (W. A. Hammond Drierite Co., Xenia, Ohio), and dry nitrogen (Matheson extra dry grade).

Periodic optical observations were made of the surface of the specimens to determine whether cracking had occurred. Once cracking was observed, the number of cycles were recorded. Cyclic loading was then continued.

The following chapter lists the results of this investigation.  
The discussion and conclusions follow.

## CHAPTER VI

### EXPERIMENTAL RESULTS

#### 6.1 General

The results of this investigation are classified under the following major headings: tests in the field-emission microscope, cathodic protection and electric fields, and cyclic loading tests. The results are summarized in Tables I, II and III, and in Figs. 16, 17 and 18.

#### 6.2 Tests in the Field-Emission Microscope

##### 6.2.1 Thermal Etching

An interesting phenomenon which was observed during the initial tests in the field-emission microscope was that U-10<sup>W</sup>/o Mo etches thermally, even at room temperature, see Fig. 9. Thermal etching, or thermal grooving is a direct result of surface energy parameters (30).

Thermal grooving was a great aid in the metallographic studies of U-10<sup>W</sup>/o Mo, in that it readily revealed the grain structure. It is strongly believed, however, that thermal grooving might be deleterious to the stress-corrosion cracking behavior of the alloy. A microscopic groove will increase local stresses, and the coalescence of dislocations at thermally-grooved boundaries may very well produce a combination of incipient cracks and locally enhanced corrosion.

Thermal grooving was not investigated further in this work. However, further research into this subject would be desirable.

### 6.2.2 Dry Tests

A. Effect of Heat Treatment - Critical Stress. The effects of heat treatment on the stress-corrosion cracking of U-10<sup>W</sup>/o Mo were studied using pure, dry oxygen, as described in Section 5.2.2B. The results are summarized in Table I.

The results shown in Table I indicate that a stress-relief anneal (with retained, large  $\approx 200\mu$  grains) improved the ductility of the specimens, but did not affect the stress-corrosion cracking behavior. Microcracks in annealed specimens were observed at 21,500 psi, and reduced fracture strengths were observed at 22,000 psi. In every case, periodic metallographic examination revealed that cracking was preceded by dulled surfaces and local corrosion.

The specimens that were given a gamma-stabilization treatment and which had a reduced grain size ( $\approx 50\mu$ ) displayed a marked improvement in stress-corrosion cracking behavior. Compared with the annealed specimens, the specimens that were given a gamma-stabilization treatment exhibited fewer cracks, and normal fracture strengths (135,000 psi).

The specimens which were tempered after the gamma-stabilization treatment exhibited the best stress-corrosion cracking behavior when compared with the specimens discussed above. No cracks were observed below 37,000 psi, and fracture strengths were in the range of 130,000 to 135,000 psi.

Under the conditions of a gamma-stabilization treatment (gamma-homogenization followed by a low temperature quench) and subsequent tempering, a tentative "critical stress", for loading in pure, dry

oxygen, was set at 36,500 psi. However, slight deviations from the conditions discussed above lowered this stress to very low values. Specimens Nos. 9 and 13 of Table I illustrate this phenomenon. Specimen No. 9, with duplex grain structure ( $\sim 200\mu$  and  $\sim 50\mu$ ) which had been gamma-stabilized and tempered, cracked along the grain boundaries of the larger grains at stresses as low as 22,000 psi, in the presence of pure, dry oxygen. A similarly treated set of specimens (No. 13), with uniform grain structure, was cold worked by drawing (10 percent reduction). After 24 hours exposure to dry oxygen, at 32,000 psi, numerous micro-cracks were observed. Periodic metallographic examination revealed that cracking, in all the cases described above, was intergranular, and always was preceded by a dulling of the surface followed by concurrent appearance of slip lines and corrosion concentrations.

Once the effects of heat treatment were evaluated, it was decided that the specimens to be used in subsequent tests were to be gamma-stabilized and tempered, and stress levels would be set at 36,000 psi, unless otherwise required in a particular test. It was expected that these heat treatments would result in excellent metallurgical properties of strength and ductility for U-10<sup>w</sup>/o Mo specimens, and that the stresses would be below the "critical stress" for tests in oxygen.

B. Effect of Dry Ambient Atmospheres. The effects of dry ambient atmospheres on the stress-corrosion cracking of U-10<sup>w</sup>/o Mo are summarized in Table I.

1. Oxygen. Metallographic examination of U-10<sup>w</sup>/o specimens tested in pure, dry oxygen revealed that the specimens had

suffered profuse surface cracking. Cracks were intergranular, and were preceded by slip line formation, and corrosion concentrations. Coalescence of slip bands and microcrack nucleation are shown on Figs. 10 (600X) and 11 (600X). Intergranular cracking in U-10<sup>W</sup>/o Mo is shown on Fig. 12 (800X). All of the specimens shown had been exposed to pure, dry oxygen.

Reloading of the specimens in vacuum after 24 hours exposure to pure, dry oxygen and pulling to failure resulted in ductile failures (percent reduction in area > 60 percent), and normal fracture strengths (130,000 psi). Reloading of specimens in pure, dry oxygen resulted in brittle fractures and reduced strengths.

2. Hydrogen. Cracking of U-10<sup>W</sup>/o Mo in pure, dry hydrogen was found to be transgranular. Fracture strengths of specimens reloaded in vacuum were in the range of 120,000 to 130,000 psi, but the ductility was reduced considerably (percent reduction in area  $\approx$  25 percent). Periodic metallographic examination of the specimens revealed that dull surfaces always preceded cracking.

3. Nitrogen, Carbon Dioxide and the Inert Gases. Nitrogen and carbon dioxide did not cause stress-corrosion cracking in the U-10<sup>W</sup>/o Mo specimens tested. Surfaces were unaffected during the tests, except for a slight tarnishing at higher

(70,000 psi) stress levels. Fractures were ductile, and fracture strengths were in the range of 130,000 to 135,000 psi.

The results of the tests with helium and argon (Table I) indicate that the specimens tested suffered a general loss in ductility similar to that observed in the tests with pure, dry hydrogen. No surface cracks were observed (1200X) prior to final catastrophic failure which occurred at stress levels ranging between 36,000 and 126,000 psi.

#### 6.2.3. Wet Tests

The combined effects of water vapor and other gases on the stress-corrosion cracking behavior of U-10<sup>W</sup>/o Mo are summarized in Table II. Specimens used in these tests were given a gamma-stabilization treatment followed by a tempering treatment as described in Section 5.2.2A.

##### A. Effect of Water Vapor.

1. Oxygen. Departure from dry conditions in tests with oxygen caused cracking of U-10<sup>W</sup>/o Mo specimens to be of a mixed nature. Both intergranular and transgranular cracks were observed, with the number of transgranular cracks increasing with increasing water vapor content.

Both ductility and fracture strengths decreased with increasing water vapor content. Periodic metallographic examination of some of the specimens revealed that surface

tarnishing, slip bands, and corrosion concentrations preceded cracking in these tests.

Fig. 13 shows the general surface deterioration of a U-10<sup>W</sup>/o Mo specimen exposed to oxygen (400X) saturated with water vapor (0.6 normalized partial pressure of water vapor\*). Fig. 14 (600X) shows corrosion products concentrated at the intersection of two slip systems, on the surface of the same specimen. Fig. 15 (600X) shows both intergranular and transgranular cracks on the surface of a specimen exposed to oxygen saturated with water vapor (0.6 normalized partial pressure of water vapor).

2. Hydrogen. The surface cracks observed on U-10<sup>W</sup>/o Mo specimens during the tests with hydrogen saturated with water vapor were transgranular. Fracture strengths and ductility were reduced.

3. Nitrogen and Carbon Dioxide. Contrary to the dry nitrogen and dry carbon dioxide tests, exposure of U-10<sup>W</sup>/o Mo specimens to nitrogen and carbon dioxide saturated with water vapor not only caused surface cracking, but the fracture parameters of the specimens reloaded in vacuum were affected as well.

Cracking observed during exposure of the specimens to saturated nitrogen was transgranular; fracture strengths and ductility were reduced.

---

\*Water vapor partial pressure normalized to one atmosphere.

Cracking observed during exposure of the specimens to saturated carbon dioxide was both transgranular and intergranular. Fracture strengths and ductility were reduced also.

B. Corrosion Products Observed. Accurate determination of corrosion products may be accomplished by means of chemical analysis and by means of X-ray techniques. Exact determination of the corrosion products observed in this investigation is beyond the scope of this work; however, a few remarks pertaining to optical observations of the corrosion products in the wet tests are made below.

The corrosion products observed during the wet tests had the appearance and consistency of the following compounds (83):

- a.  $UO_4 \cdot 2H_2O$  -- an apparently adherent pale yellow tarnish.
- b.  $UO_2$  -- a non adherent tarnish and scaly compound ranging in color from light brown to dark brown to black. The darkest portions were severely cracked.
- c.  $UO_3$  -- slight traces of a light red compound.

#### 6.2.4 Time-to-Fail Tests

The time-to-fail tests were designed to investigate the behavior of U-10<sup>W</sup>/o Mo specimens subjected to a constant load in a particular environment. The specimens used in these tests were either "as-received", annealed, or gamma-stabilized and tempered, and were exposed to either dry oxygen, oxygen saturated with water vapor, dry hydrogen, or hydrogen saturated with water vapor.

Figure 16 shows a graph of load vs. time to fail, in pure, dry oxygen, of U-10<sup>W</sup>/o Mo specimens in three distinct conditions: "as-received", annealed, and gamma-stabilized and tempered. It may be noted on Fig. 16 that "as-received" specimens exhibited the shortest times to fail, whereas the tempered specimens exhibited the longest times, as would be expected from the results of Table I.

Figure 17 summarizes the combined effect of water vapor and oxygen on the time to fail of U-10<sup>W</sup>/o Mo specimens. The curves are plots of normalized partial pressure of water vapor vs. time to fail, with stress as a parameter. It may be noted on Fig. 17 that increasing the water vapor content shortens the times to fail. Increasing the stress level shortens the times to fail also.

The combination of hydrogen and water vapor was the most dangerous to U-10<sup>W</sup>/o Mo, in agreement with the results of Table II. Figure 18 shows a graph of load vs. time to fail for U-10<sup>W</sup>/o Mo specimens tested in wet hydrogen (0.2 normalized partial pressure of water vapor). These tests demonstrated, once more, that hydrogen and water vapor were deleterious to U-10<sup>W</sup>/o Mo.

### 6.3 Cathodic Protection and Effect of Electric Fields

Tests on cathodic protection and the effect of electric fields were performed as described in Section 5.2.2C. The specimens used in these tests were gamma-stabilized and cold worked (10 percent reduction) to induce stress-corrosion cracking susceptibility. The specimens were exposed to oxygen, hydrogen, nitrogen, and carbon dioxide, both dry and

saturated with water vapor. The specimens tested under these conditions were found to contain concentrated corrosion products and profuse surface cracking similar to those observed during the tests in the field-emission microscope, see Section 6.2.

No protection from stress-corrosion cracking was found possible for the U-10<sup>W</sup>/o Mo specimens tested using the techniques of cathodic protection and electric fields.

#### 6.4 Cyclic-Loading Tests

The cyclic-loading tests made on U-10<sup>W</sup>/o Mo specimens were performed using the apparatus shown in Fig. 8, and described in Section 5.2.2D. The specimens used were gamma-stabilized and tempered, and were subjected to cyclic loads of 36,000 psi in tension. Some specimens were tested in ambient air (air conditioned room at 72°F and 40 percent R.H.) and other specimens were tested using either dry, laboratory air, or dry nitrogen as "gaseous shields". The results are summarized in Table III.

Surface cracks were observed (60X) on U-10<sup>W</sup>/o Mo specimens exposed to ambient air, after only 20 cycles of loading. This value was slightly increased to 30 cycles when the specimens were exposed to dry, laboratory air. Nitrogen-bathed specimens, on the other hand, appeared to be free of cracks (1200X) even after 1000 cycles.

Figure 19 shows two photomicrographs taken during a cycle-loading test in dry, laboratory air. The photomicrographs (160X), taken 10 cycles apart, show surface cracking believed to occur through the coalescence of dislocations (see thermal etch pits on Fig. 19) which arrive at the surface.

### 6.5 Summary

The results of this investigation suggest that stress-corrosion cracking of U-10<sup>W</sup>/o Mo can be either intergranular, transgranular, or both, depending on the specific ambient atmosphere which prevails in a particular test. In this respect, it appears that wet hydrogen is most dangerous to U-10<sup>W</sup>/o Mo in that the alloy is not only embrittled, but weakened as well.

Heat treatment appears to have a definite bearing on the stress-corrosion cracking of U-10<sup>W</sup>/o Mo, whereas cathodic protection and electric fields do not.

A dry nitrogen environment prevented the stress-corrosion cracking of U-10<sup>W</sup>/o Mo specimens subjected to cyclic tensile loads with maximum stress amplitudes of 36,000 psi. A dry nitrogen environment, no doubt, serves as a "protective shield".

## CHAPTER VII

### DISCUSSION AND CONCLUSIONS

#### 7.1 Tests in the Field-Emission Microscope

##### 7.1.1 Heat Treatment - Critical Stress

The stress-corrosion cracking behavior of U-10 <sup>w</sup>/<sub>o</sub> Mo was directly influenced by heat treatments. The results shown in Table I and Fig. 16 indicate that the best stress-corrosion cracking behavior of the specimens tested was obtained using a gamma homogenization and quench (gamma-stabilization treatment) followed by a tempering treatment as described in Section 5.2.2A. The benefits of retaining a gamma-structure need no further discussion. The tempering treatment relieves the cooling stresses induced during the gamma-stabilization treatment, and in addition, precipitates some alpha-phase, which does not coalesce (75).

Dislocations as well as subgrain and grain boundaries provide nucleation sites for alpha-precipitation (84). The alpha-precipitation may inhibit gross plastic flow by locally pinning dislocations. Locally stopped dislocations possibly prevent pile-ups which in turn reduce stress concentrations at the surface. Reduced surface stress concentrations may be responsible for reduced corrosive action on the surface.

A very close control of heat treatment and processing techniques are necessary for U-10 <sup>w</sup>/<sub>o</sub> Mo since slight deviations from the

techniques discussed above tend to induce enhanced stress-corrosion cracking susceptibility.

The critical stress, which was set at 36,500 psi on the basis of the results obtained in the tests with pure, dry oxygen, discussed in Section 6.2.2A, should not be relied upon as an engineering design parameter. This stress value was obtained only for U-10 <sup>W</sup>/<sub>0</sub> Mo specimens under special circumstances of careful heat treatment. It cannot be overemphasized that slight deviations from the techniques described above may cause cracking at stress levels considerably lower than 36,500 psi.

#### 7.1.2 Dry Tests

A. Oxygen. Cracking due to pure, dry oxygen was found to be intergranular in nature, see Table I. Metallographic observations revealed that cracking was preceded by slip bands and corrosion concentrations along grain boundaries. The inception of stress-corrosion cracking in U-10 <sup>W</sup>/<sub>0</sub> Mo exposed to pure, dry oxygen, then, was thought to occur through the pile-up of dislocations along grain boundaries. This produced a state of stress concentration which, assisted by enhanced corrosion activity, promoted the generation of microcracks, see Figs. 10, 11, and 12.

Intergranular cracking of U-10 <sup>W</sup>/<sub>0</sub> Mo in pure, dry oxygen suggests that cracking may be due to the corrosion susceptibility of the alloy, assisted by the stresses present, both residual and applied.

Oxygen may play a dual role in the stress-corrosion cracking of U-10 <sup>W</sup>/<sub>0</sub> Mo. It may not only act as the chemical agent responsible

for the oxidation process, but also may act as a mechanical wedge, in the form of  $UO_2$ , in promoting cleavage. Differences in epitaxy, due to differences in lattice constants between the base metal and the oxide, in uranium, give rise to coherency stresses (85) of sufficient magnitude to cause crack initiation and subsequent discontinuous failure of the metal. Chirigos (85) states that the mismatch or disregistry between base metal (U) and the oxide ( $UO_2$ ) is approximately 11%, corresponding to lattice constants of 3.47 and 5.47 angstroms, respectively.

B. Hydrogen. The U-10  $\frac{w}{o}$  Mo specimens tested in pure, dry hydrogen were susceptible to hydrogen embrittlement or hydrogen-stress cracking. Cracking of U-10  $\frac{w}{o}$  Mo in pure, dry hydrogen was found to be transgranular, see Table I. The surface of the specimens was characterized by the absence of slip bands, and the tests revealed a general loss of ductility. Several mechanisms have been proposed to explain hydrogen embrittlement (34); however, at this time it is impossible to suggest which mechanism may have been operative in the U-10  $\frac{w}{o}$  Mo specimens tested.

C. Nitrogen and Carbon Dioxide. Dry nitrogen and dry carbon dioxide did not promote surface cracking of the U-10  $\frac{w}{o}$  Mo specimens tested. This prompted the use of dry nitrogen as a protective "gas shield" in the cyclic-loading tests.

D. Helium and Argon. The data on Table I for helium and argon show that the U-10  $\frac{w}{o}$  Mo specimens tested in these gases displayed brittle fractures at stress levels which ranged between 35,500 and 126,000 psi. Catastrophic failure of the specimens tested in inert

atmospheres took place without any prior notice; that is, no surface cracks were apparent (1200X) prior to final fracture. The absence of surface cracks prior to final failure suggests that fracture may have started from within the specimens, with catastrophic failure ensuing in a relatively short time.

A comparison between specimens Nos. 25 and 26, Table I, (loaded in tension in atmospheres of tank argon and argon passed through Drierite and copper foil trap, respectively, see Section 5.2.2B) suggests that the tank argon used was probably contaminated with water vapor as suggested by Gorman (82). This would account for the lower fracture strengths of specimen No. 25. This was in agreement with the results obtained, in this investigation, in tests with water vapor and other gases, see Table II.

The special condition of no surface cracks prior to failure, and embrittlement displayed by U-10 <sup>w</sup>/<sub>o</sub> Mo specimens in the inert atmospheres suggest that there existed an embrittling mechanism in which fracture began from within the specimens. This mechanism may be similar to that of hydrogen embrittlement. The tests with the inert gases were not pursued further. It is clear that the results obtained with helium and argon are inconclusive, and warrant further investigation.

### 7.1.3 Wet Tests

The results shown on Table II indicate that water vapor was responsible for reduced strengths and brittle behavior of the specimens tested, and that increasing the water vapor content of the atmosphere promoted transgranular cracking.

Interesting results were obtained with carbon dioxide in which cracking was found to be of a mixed nature. No definite conclusions were drawn, except that the water vapor contributed to lowering the fracture strength and the ductility of the specimens.

The data on Table II and Fig. 17 suggest that high water vapor concentrations must be avoided, and that design stresses should be kept below 36,500 psi.

Of all the different combinations of dry gases and water vapor that were studied, wet hydrogen was the most dangerous and should be avoided.

The transgranular cracking of U-10 <sup>W</sup>/<sub>0</sub> Mo specimens, which accompanied the tests with the gases saturated with water vapor, is believed to be due to mechanical failure of the alloy with corrosion assisting the process of fracture. The role of the water vapor may have been that of weakening the metallic bonds, perhaps through some surface-energy reduction mechanism.

### 7.2 Cathodic Protection and Electric Fields

Cathodic protection and electric fields had no effect on the stress-corrosion cracking behavior of the U-10 <sup>W</sup>/<sub>0</sub> Mo specimens tested. The results of the tests designed to evaluate cathodic protection and the effect of electric fields indicated that these simple protective techniques are not effective in protecting U-10 <sup>W</sup>/<sub>0</sub> Mo from stress-corrosion cracking.

### 7.3 Dry Nitrogen as a Protective Shield

The results obtained from the cyclic-loading tests on U-10 <sup>W</sup> /o Mo, Table III, suggest that pure, dry nitrogen may be used as a "protective shield" during cyclic loading of U-10 <sup>W</sup> /o Mo in ambient air.

### 7.4 Design Considerations

In the light of the results obtained in this investigation, it is suggested that structural members made from U-10 <sup>W</sup> /o Mo should be given a gamma-stabilization treatment and a tempering treatment prior to initial loading of the structure. The heat treatments should be closely controlled to insure a uniform grain structure of medium sized grains ( $\approx 50 - 100 \mu$ ).

Design stresses should be kept below 36,500 psi, and the relative humidity of the ambient atmosphere should be constantly kept at a practical minimum.

Finally, the structure should be shielded from the ambient atmosphere, during loading, with a stream of dry nitrogen.

### 7.5 Conclusions

The major conclusions that were drawn from this work are the following:

- a. The U-10 <sup>W</sup> /o Mo specimens tested were susceptible to stress-corrosion cracking in pure, dry oxygen. The stress-corrosion cracking susceptibility of the specimens was directly affected by heat treatments. The greatest resistance to stress-corrosion cracking observed in this

investigation resulted from a heat treatment of the specimens which included a gamma-stabilization treatment followed by a tempering treatment. With specimens heat treated in this manner, it was possible to obtain a "critical stress" value of 36,500 psi. This value of stress was highly susceptible to slight deviations from the heat treatments described, and should not be relied upon for design purposes.

b. The U-10 <sup>w</sup>/<sub>o</sub> Mo specimens tested were susceptible to hydrogen embrittlement.

c. The stress-corrosion cracking problem in U-10 <sup>w</sup>/<sub>o</sub> Mo was worsened by the presence of water vapor in the ambient atmospheres.

d. Cracking of U-10 <sup>w</sup>/<sub>o</sub> Mo was either intergranular, transgranular, or both, depending upon the particular atmosphere which prevailed during a test. Pure, dry oxygen caused intergranular cracks while pure, dry hydrogen caused transgranular cracks. The presence of water vapor promoted transgranular cracking which became more severe with increasing water vapor content of the atmospheres.

e. Pure, dry nitrogen and pure, dry carbon dioxide did not cause stress-corrosion cracking in the U-10 <sup>w</sup>/<sub>o</sub> Mo specimens tested. These gases, however, saturated with water vapor, did cause stress-corrosion cracking. The stress-corrosion cracking observed was attributed to the presence of water vapor.

- f. Tests with helium and argon were inconclusive.
- g. The U-10 <sup>W</sup>Mo specimens tested were not protected from stress-corrosion cracking through the use of cathodic protection techniques.
- h. A dry nitrogen atmosphere served as a "protective shield" to U-10 <sup>W</sup>Mo specimens which were loaded cyclically in tension.

## CHAPTER VIII

### RECOMMENDATIONS FOR FUTURE RESEARCH

#### 8.1 Alpha-Phase Precipitation

The effect of heat treatment was shown, in this investigation, to be a factor of major consideration in the stress-corrosion cracking of the U-10<sup>W</sup>/o Mo specimens tested. Furthermore, it appears, from these studies, that some phase precipitation, resulting from the tempering treatment, may be beneficial in reducing the stress-corrosion cracking susceptibility of this alloy.

Further studies of the effect of the alpha-phase should be conducted to include quantitative measurements of the amount of alpha precipitated and its correlation with stress-corrosion cracking. These studies should not only include metallographic examinations, but also X-ray diffraction and electron microprobe techniques.

#### 8.2 Corrosion Studies

The results of this investigation suggested that intergranular cracking of the U-10<sup>W</sup>/o Mo specimens tested was due to enhanced corrosion with stress assisting the process of fracture, and that transgranular cracking was due to mechanical failure with corrosion assisting the process of fracture. However, no indications were obtained as to the exact mechanism of corrosion that was operative in each case.

It is believed that further understanding of the stress-corrosion cracking of U-10<sup>W</sup>/o Mo may be gained from studies aimed at determining the corrosion mechanisms which contribute to each type of cracking.

### 8.3 Electropolishing and Hydrogen Pick-Up

Hydrogen embrittlement is a serious consideration in the use of U-10<sup>W</sup>/o Mo. A large probability exists that some hydrogen may be introduced into the U-10<sup>W</sup>/o Mo structure during electropolishing, and it is quite possible that any hydrogen pick-up might affect the results of subsequent tests. A mass-spectrometer analysis of a heated, electropolished specimen should give an indication as to how much hydrogen may be picked up during electropolishing operations.

Electropolishing solutions that do not promote hydrogen evolution (86) should also be investigated in future studies.

### 8.4 Shot Peening

Tensile stresses are thought to be responsible for increasing the stress-corrosion cracking susceptibility of alloys (8). Surface compressive stresses, then, should improve stress-corrosion cracking behavior. One means of inducing surface compressive stresses is through shot peening. Turley, et al. (53) have studied the effect of shot peening on the stress-corrosion cracking of a 9Ni-4Co steel alloy. Their conclusions were that shot peening improved the resistance to stress-corrosion cracking in the specimens they tested.

Shot peening tests of U-10<sup>W</sup>/o Mo should be performed to determine if its resistance to stress-corrosion cracking is improved.

#### 8.5 Effect of Inert Atmospheres

The results of the tests of U-10<sup>W</sup>/o Mo in helium and argon were reported, in this investigation, to be inconclusive. A definite explanation should be given to the embrittling phenomena that were observed. It was suggested that perhaps a mechanism similar to hydrogen embrittlement may have been responsible for the brittle behavior of the specimens tested. In this respect, mass-spectrometer tests of heated specimens previously in contact with the inert gases should give an indication as to whether any gas was entrained.

## APPENDIX A

### PARTIAL DISLOCATIONS AND THE STACKING FAULT

In the hard-sphere model, a perfect crystal is visualized as an infinite array of carefully stacked layers of spheres with a characteristic number of nearest neighbors. The order of sequence of the atom layers in the stack, known as the stacking sequence (89), is referred to by fixing one layer as an A layer, and all other layers with atoms in identical positions as A layers also. Layers of atoms in other positions in the stack are referred to as B, C, D layers, etc.

In contrast to the ideal, actual crystals possess many imperfections which result in regions of misfit. In some of these regions of misfit the ideal stacking sequence is altered. The altered stacking sequence is called the stacking fault (89). Stacking faults are surface defects which have a characteristic energy per unit area called the stacking fault energy.

More commonly, the term "stacking fault" is associated with faults which result from the dissociation of unit dislocations into partial dislocations, or from the precipitation of one or more layers of point defects (i.e., vacancies or interstitials). The dissociation of a unit dislocation into partial dislocations is energetically favorable, as will become apparent below.

The concept of the stacking fault, which arises from the dissociation of unit dislocations into partial dislocations, is more easily

visualized in the face-centered cubic crystalline system, than in either the hexagonal close-packed or the body-centered cubic system. The fcc system will be used to illustrate the stacking fault concept, which will then be extended to the bcc system.

The primary slip planes in the fcc lattice are the octahedral  $\{111\}$  planes (30). The view of Fig. 20 is normal to a plane of this type. This figure shows a unit dislocation in the edge orientation. The darkened circles represent the close-packed  $(111)$  plane at which the extra plane of the dislocation ends, while the white circles are the atoms in the next following close-packed  $(111)$  plane. The zigzag row of atoms which is missing corresponds to the missing plane of the dislocation.

Movement, to the right, of the atoms immediately to the left of the missing plane, through the horizontal distance  $b$ , displaces the dislocation one unit to the left. The vector  $b$  represents the Burgers vector of the dislocation. Similar movements in succession, of the planes of atoms that find themselves to the left of the dislocation, will cause the dislocation to move across the entire crystal.

Normally, motion of a dislocation such as shown in Fig. 20 through the horizontal distance  $b$  would involve a very large strain because each white atom at the slip plane would be forced to climb over the dark atom below it and to its right. What is actually believed to happen (30) is that the indicated plane of atoms makes the move indicated by the vectors marked  $c$  in Fig. 21. This movement can occur with a much smaller strain of the lattice. A second movement of the same

type, indicated by the vectors marked  $\underline{d}$ , brings the atoms to the same final positions as the single displacement  $\underline{b}$  of Fig. 20.

The atom arrangement of Fig. 21 is particularly significant because it shows how a single-unit dislocation can break down into a pair of partial dislocations. The isolated, single zigzag row of atoms has an incomplete dislocation on each side of it. The Burgers vectors of these dislocations are the vectors  $\underline{c}$  and  $\underline{d}$  shown in Fig. 21.

When a total dislocation breaks down into a pair of partials, the strain energy of the lattice is decreased. This occurs because the energy of a dislocation is proportional to the square of its Burgers vector, and because the square of the Burgers vector of the total dislocation is more than twice as large as the square of the Burgers vector of a partial dislocation.

Because the partial dislocations of Fig. 21 represent approximately equal lattice strains (30), a repulsive force exists between them which forces the partials apart. Such a separation will add additional planes of atoms to the single zigzag plane of Fig. 21, as shown in Fig. 22.

The white atoms that lie between the two partial dislocations shown in Fig. 22 have stacking positions which differ from those of the far side of either of the partials. Thus, assuming that the dark atoms occupy A positions in a stacking sequence, and the white atoms at either end of the figure, B positions, (normal stacking for fcc is ABCABC), then the white atoms between the two partial dislocations lie on C positions. The discontinuity which results causes the following "stacking fault": ACABCA.

There is an interfacial energy associated with a stacking fault. This stacking fault energy plays an important part in determining the distance of separation between the partials. The larger the separation between the partial dislocations, the smaller the repulsive force between them. On the other hand, the total surface energy associated with the stacking fault increases with the distance between partial dislocations. The separation between the two partials, thus, represents an equilibrium between the repulsive energy of the dislocations and the surface energy of the fault.

In the body-centered cubic lattice, there is no close-packed plane. The most nearly close-packed plane is the (110) on which most of the slip is thought to occur (28).

Figure 23 shows the atomic arrangement of two adjacent (110) planes. The stacking sequence of this type of planes is ABABAB. Unlike the stacking of close-packed planes in the fcc system, the positioning of one (110) plane over another is unique. However, there are two sites into which atoms in the upper layer can move in order to decrease the spacing between the two planes. These non-equilibrium sites are the hollows on either side of the saddle points which are the stable equilibrium positions. The easiest path an atom moving over a (110) plane may take from one position of equilibrium to another is along the route indicated by the vectors  $\underline{b}_1$ ,  $\underline{b}_2$ , and  $\underline{b}_3$  in Fig. 23. A perfect dislocation on a (110) plane can thus split up into three partial dislocations with Burgers vectors  $\underline{b}_1$ ,  $\underline{b}_2$ , and  $\underline{b}_3$ . The process is analogous to that discussed for the fcc lattice, and, as before, the width of the split depends upon the stacking fault energy.

As pointed out above, the stacking sequence of the  $\{110\}$  type of planes of the bcc system is ABALAB. Contrary to the fcc lattice, a C type position does not exist in the bcc lattice. The stacking fault, then, results in either two A planes or two B planes opposite each other: ABAABA, or ABBAB. This, however, is energetically unfavorable (28, 90), and the proper stacking sequence is restored by shifting the planes in a direction parallel to themselves.

Very little additional information is available on the stacking fault of bcc crystals. Further research is definitely needed in this area.

TABLE I. DRY TESTS

Specimen No. 2 of each 0.010 in. and 0.020 in. Dia.	Condition	Atmos- phere	Load ksi +0.5	Appearance after 24 hrs. Exposure	Cracking	Fracture Strength ksi +0.5	Percent Reduction in Area
1	Annealed; Large grain size $\approx 200\mu$	O <sub>2</sub>	10.4	No cracks	Inter- granular	130.0	60
2	"	"	20.0	No corrosion or cracks; dull surface	"	125.0	60
3	"	"	20.5	Thermal etch pits; Localized corrosion no cracks	"	125.0	60
4	"	"	21.0	Fully developed slip lines; concentrated cor- rosion; no microcracks	"	120.0	60
5	"	"	21.5	Enhanced corrosion con- centrated at grain boundaries and slip lines, extending into grains; 2 cracks	"	130.0	55
6	"	"	22.0	Fully covered with corrosion products; many microcracks	"	43.0	30
7	$\gamma$ -stabilized small grain size $\approx 50\mu$	"	22.0	Dull surface; few micro- cracks; fully developed slip lines	"	130.0	60
7a	"	"	22.0	"	"	135.0	60

TABLE I. DRY TESTS--Continued

8	γ-stabilized and tempered; GS ~ 50μ	O <sub>2</sub>	22.0	No cracks; slip lines barely resolvable at 1200X	Intergranular	135.0	60
9	γ-stabilized and tempered duplex GS	"	22.0	Minute microcracks; corrosion apparent	"	130.0	60
10	γ-stabilized and tempered, plus GS 50μ	"	32.0	No cracks; slip lines fully developed; corrosion products unresolvable at 1200X	---	134.0	60
11	γ-stabilized and tempered	"	32.0	"	---	134.0	60
12	"	"	35.0	"	---	135.0	60
13	" plus cold worked	"	32.0	Corrosion concentrations and numerous microcracks	Intergranular	116.0	60
14	γ-stabilized and tempered	"	40.0	μ-cracks apparent at 600X	"	120.0	60
15	"	H <sub>2</sub>	36.0	Dull surface; one large crack	Transgranular	130.0	25
16	"	"	36.0	Dull surface; several microcracks	"	120.0	20
17	γ-stabilized and tempered	N <sub>2</sub>	36.0	Surface unaffected	---	135.0	60
18	"	"	70.0	Slight tarnishing	---	135.0	60
19	"	CO <sub>2</sub>	36.0	Surface unaffected	---	135.0	60

TABLE I. DRY TESTS--Continued

	Y-stabilized and tempered	CO <sub>2</sub>	70.0	Surface unaffected	---	135.0	60
20							
21	"	He	36.0	"	---	75.0	25
22	"	"	36.0	"	---	36.0	20
23	"	A	36.0	"	---	36.0	15
24	"	"	36.0	"	---	100.0	20
25	"	"	36.0	"	---	36.0	12
26*	"	"	36.0	"	---	126.0	30

\*Argon used in these tests was dried by passing through Drierite and a copper foil, glass trap.

TABLE II. WET TESTS

Specimen No. 2 of each 0.010 in. and 0.020 in. Dia.	Atmos- phere	Normalized partial pressure of water vapor	Load ksi $\pm 0.5$	Appearance after 24 hrs. Exposure	Cracking	Fracture Strength ksi $\pm 0.5$	Percent Reduction in area
A	O <sub>2</sub>	0.20	36.0	Some surface tarnish- ing, no cracks	---	120.0	45
B	"	0.20	36.0	Corrosion concentra- tions, and several microcracks	Mixed	110.0	43
C	"	0.40	None	Some corrosion; no cracks	---	128.0	40
D	"	0.40	36.0	Corrosion concentra- tions; several hair- line cracks	Mixed	128.0	40
E	"	0.60	None	Some corrosion; no cracks	---	83.0	4.8
F	"	0.60	36.0	Corrosion concentra- tions; several cracks	Mixed	90.0	4.8
G	H <sub>2</sub>	0.20	36.0	Surface tarnished; several microcracks	Trans- granular	36.0	4
H	"	0.40	36.0	"	"	36.0	4
I	N <sub>2</sub>	0.20	36.0	Surface tarnished; several microcracks	Trans- granular	36.0	40
J	"	0.60	36.0	"	"	36.0	15
K	CO <sub>2</sub>	0.20	36.0	"	Mixed	36.0	40
L	"	0.60	36.0	"	Mixed	36.0	12

TABLE III. CYCLIC-LOADING TESTS

Specimen No. 2 each 0.020 in. Dia.	Atmosphere	Percent Rel. Hum.	Load ksi $\pm 0.5$	Appearance after number of cycles
1	Ambient	30	36.0	Surface cracks apparent (60X) after 20 cycles
2 Covered with glass wool	Laboratory air passed through Drierite	---	36.0	Surface cracks apparent (60X) after 30 cycles
3 Covered with glass wool	Tank N <sub>2</sub>	---	36.0	No cracks after 1000 cycles

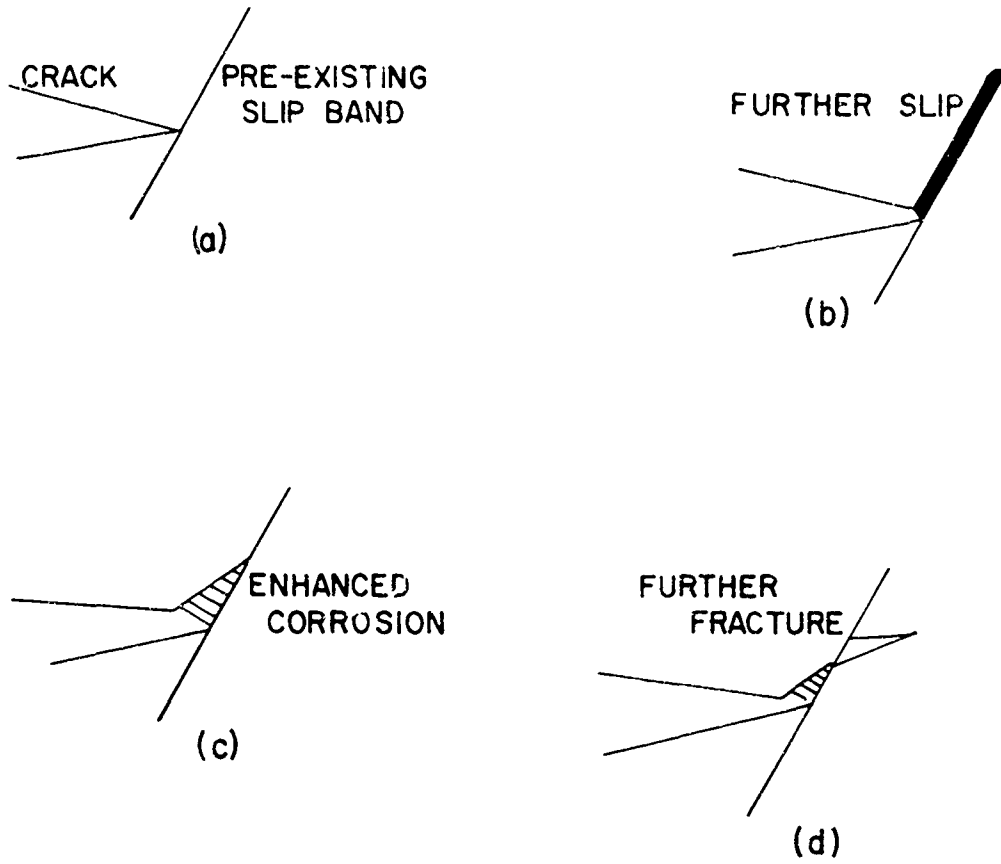


Fig. 1. Stages in the re-initiation of a crack from a slip band (24).

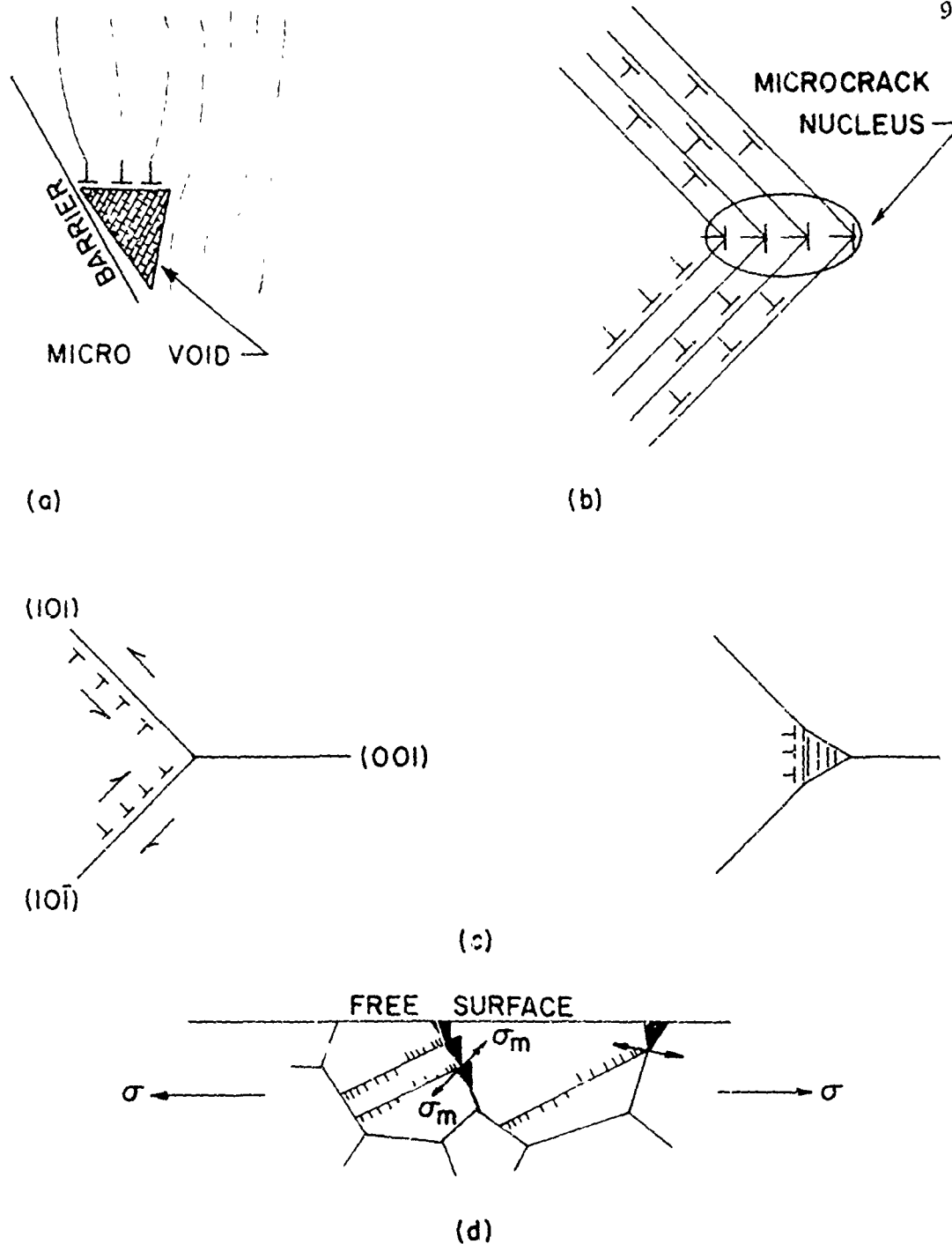


Fig. 2 Dislocation mechanisms of crack nucleation. (a) Dislocation pile-up at a barrier; (b) microcrack nucleus formed by dislocation pile-up ahead of an advancing crack; crack grows by joining with nucleus (87); (c) motion of dislocations on intersecting  $\{110\}$  planes in the bcc structure, resulting in the nucleation of a void which forms a crack on a  $\{100\}$  plane (88); (d) a model for intergranular corrosion cracking (11).

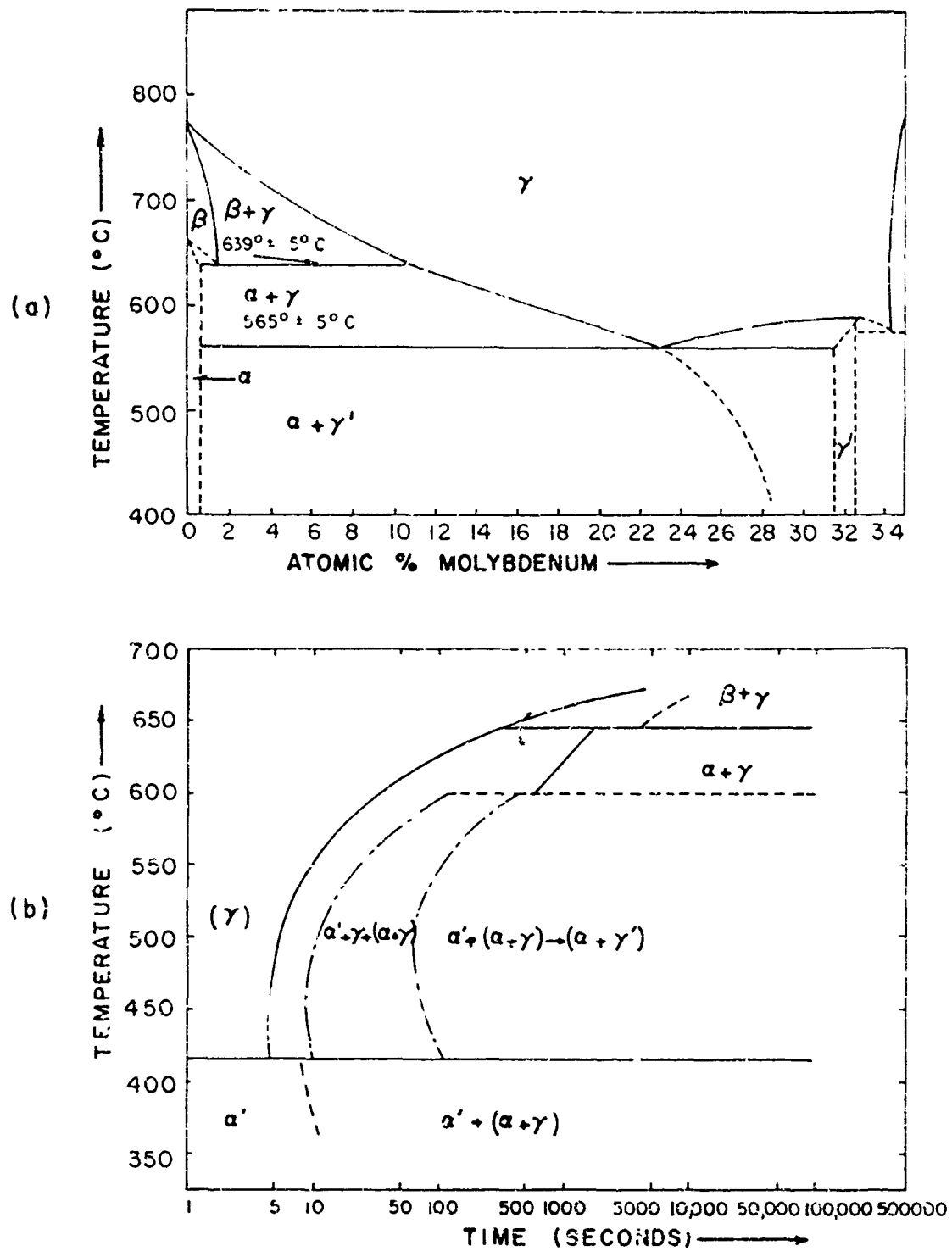


Fig. 3. (a) Equilibrium diagram of the uranium-molybdenum alloy system (73).

(b) TTT diagram of a U-2.5% Mo alloy as determined by metallography and hardness tests (74).

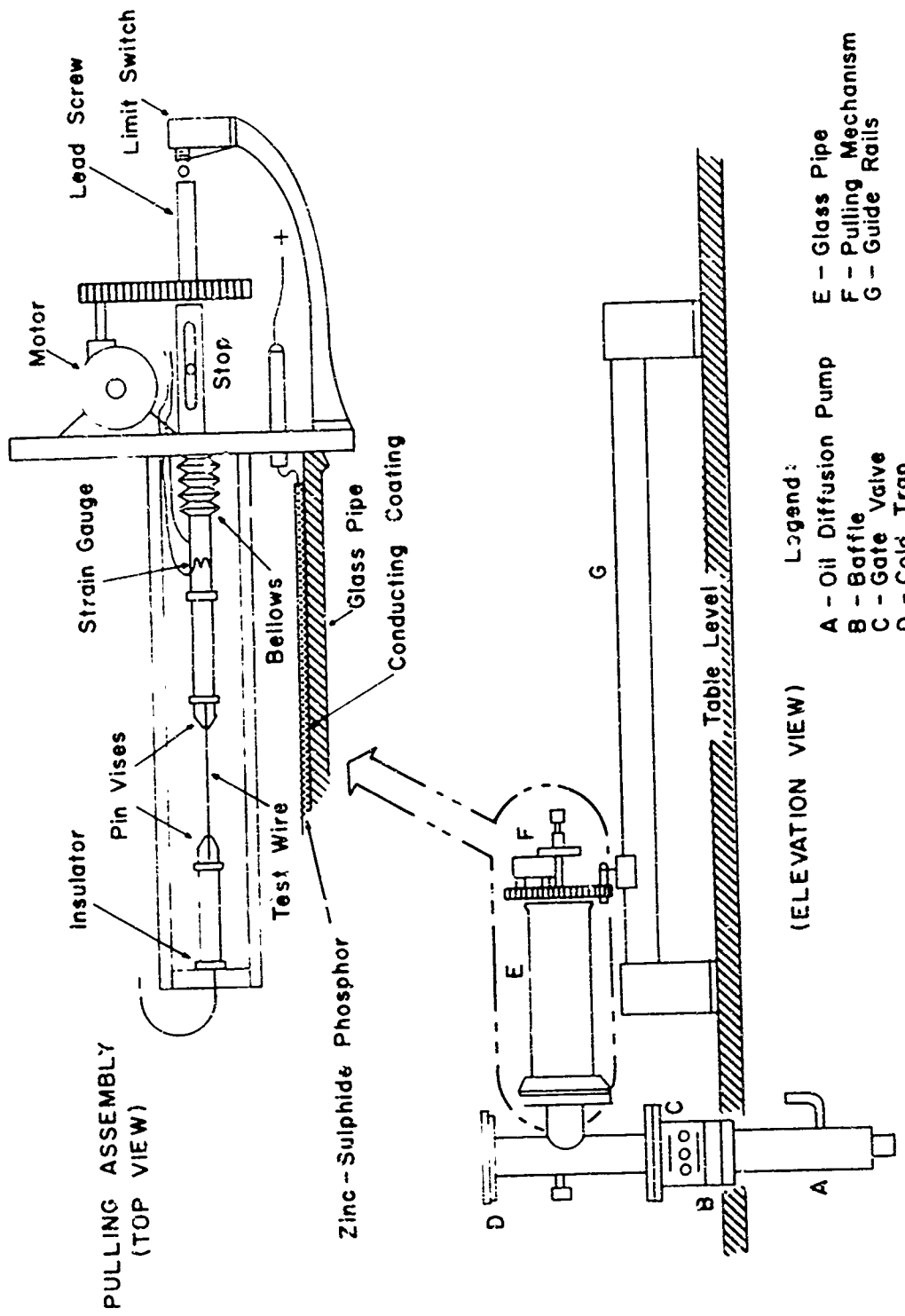


Fig. 4. Cylindrical field-emission microscope for wire studies.

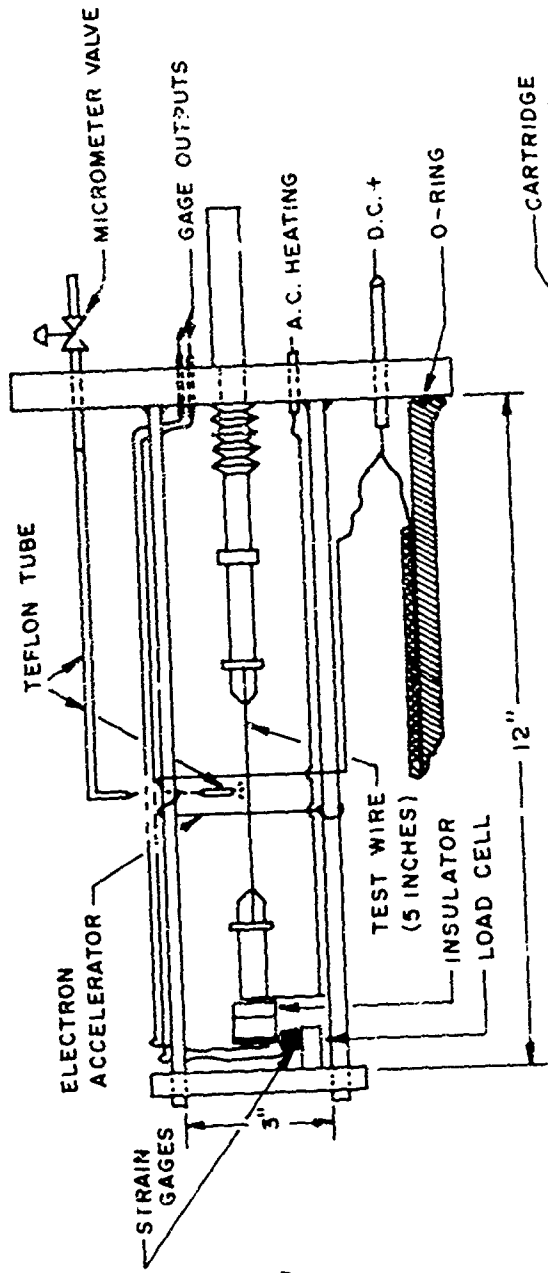


FIG. 5a  
MODIFIED PULLING  
ASSEMBLY

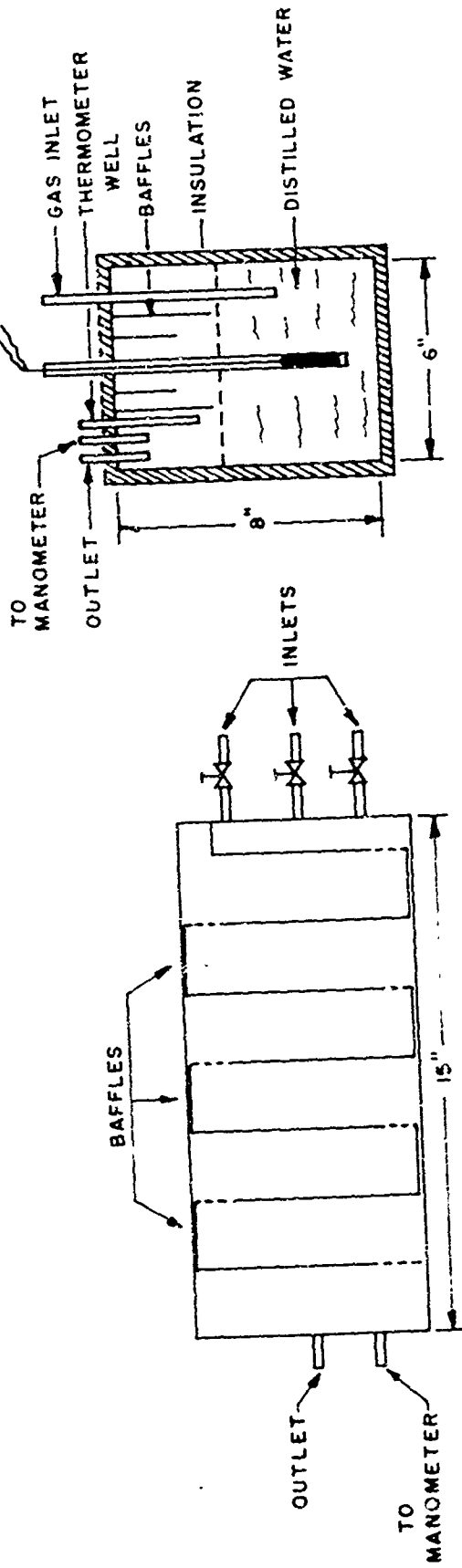


FIG. 5b GAS MIXING CHAMBER

FIG. 5c GAS WASHER TANK

Fig. 5. Modified Field-Emission Microscope pulling assembly; gas mixing chamber and gas washer tank.

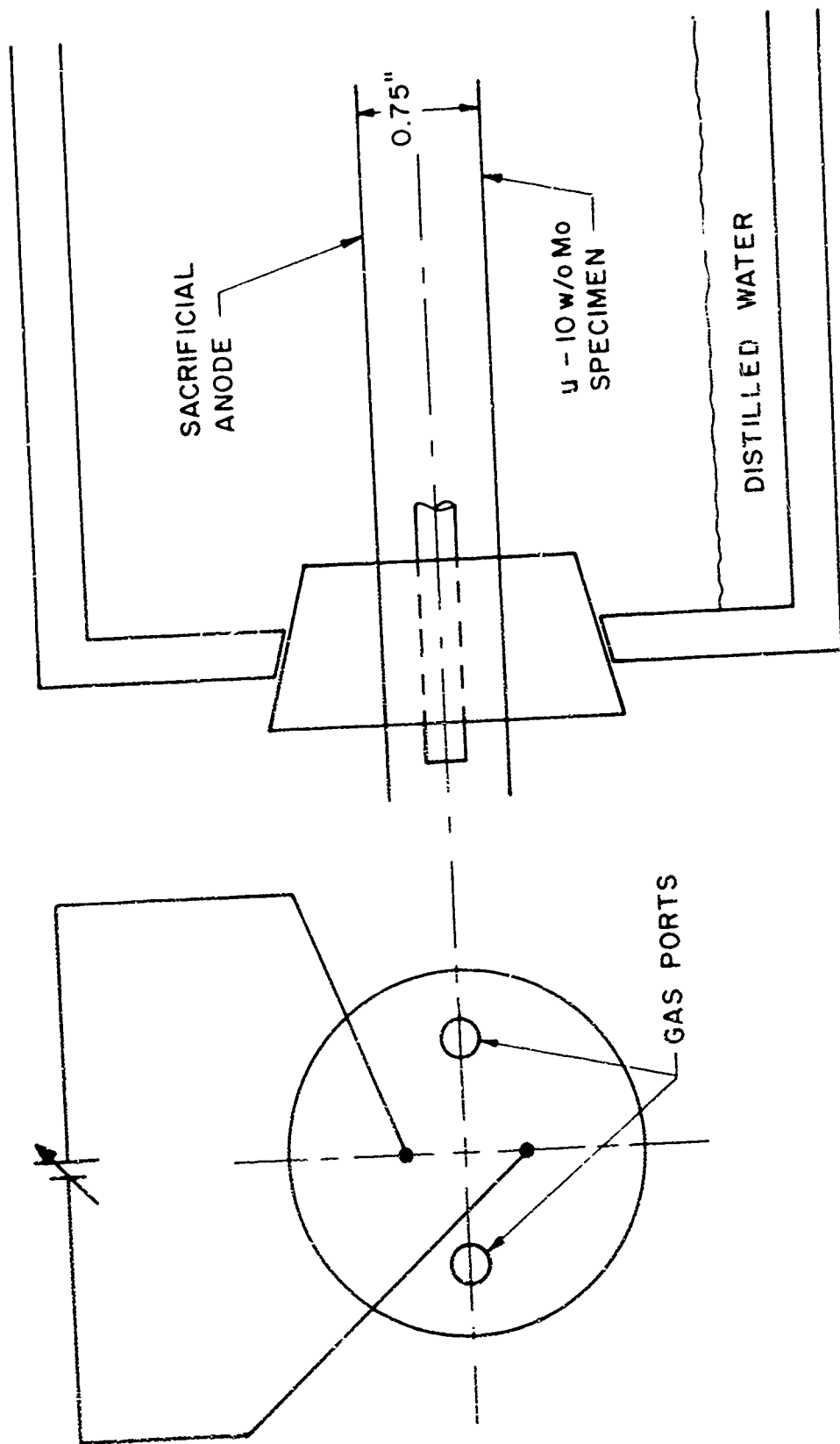


Fig. 6. Cathodic protection apparatus and electric circuit.

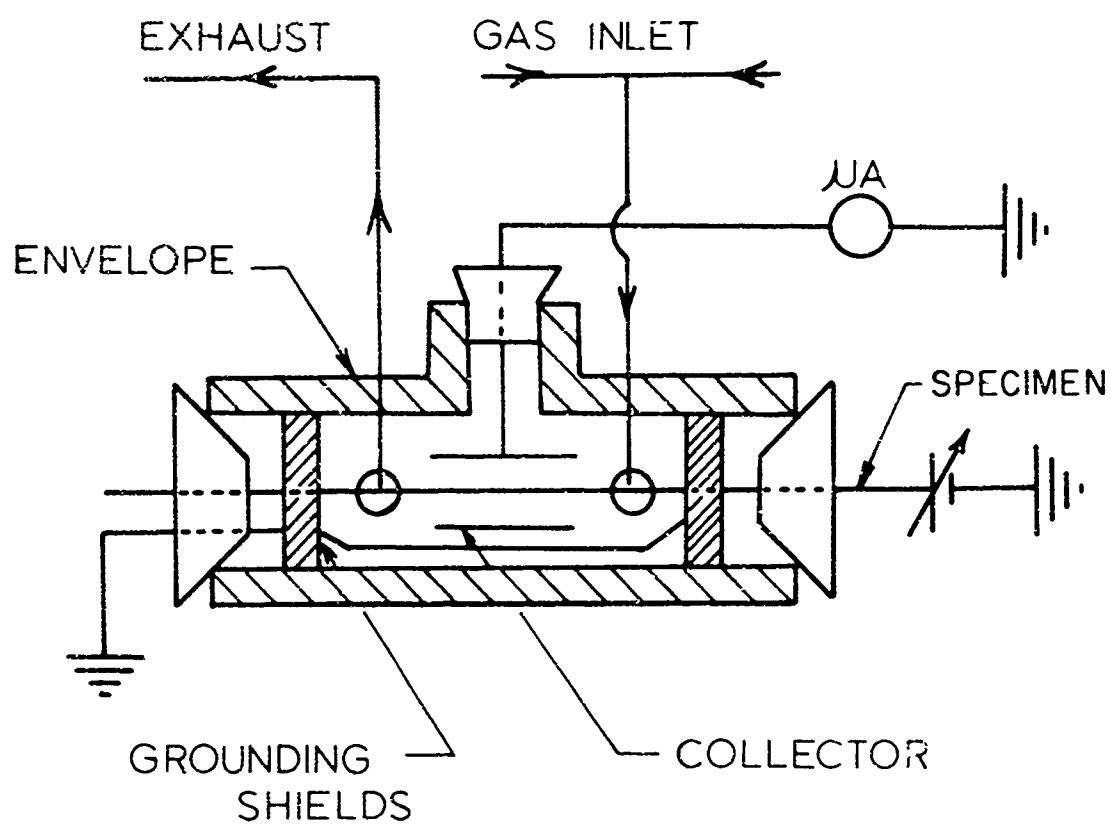


Fig. 7. Static, electric fields apparatus and electric circuit.

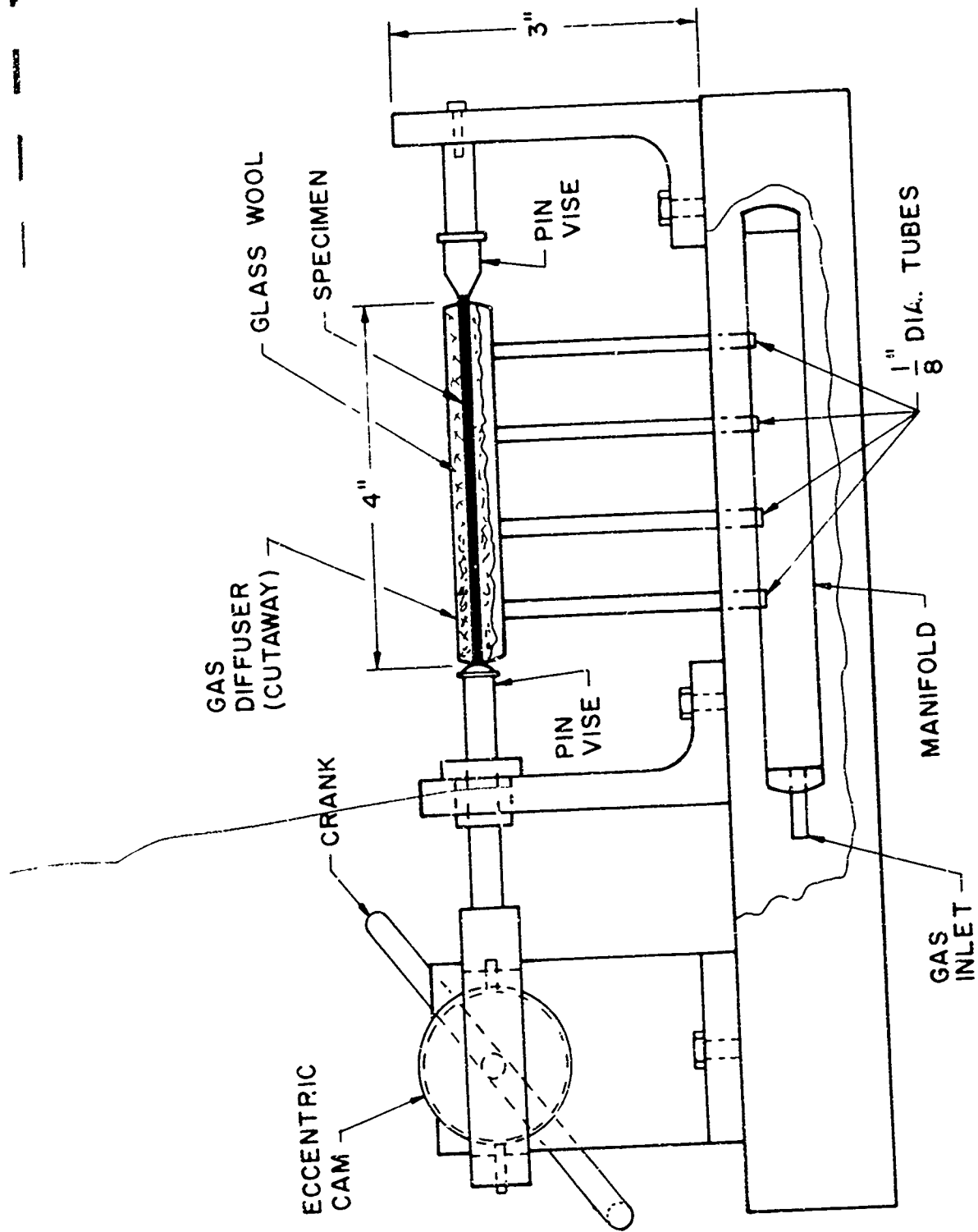


Fig. 8. Cyclic-loading apparatus.



Fig. 9. Thermal grooving and etch pits in a U-10<sup>W/o</sup> Mo specimen (400X).

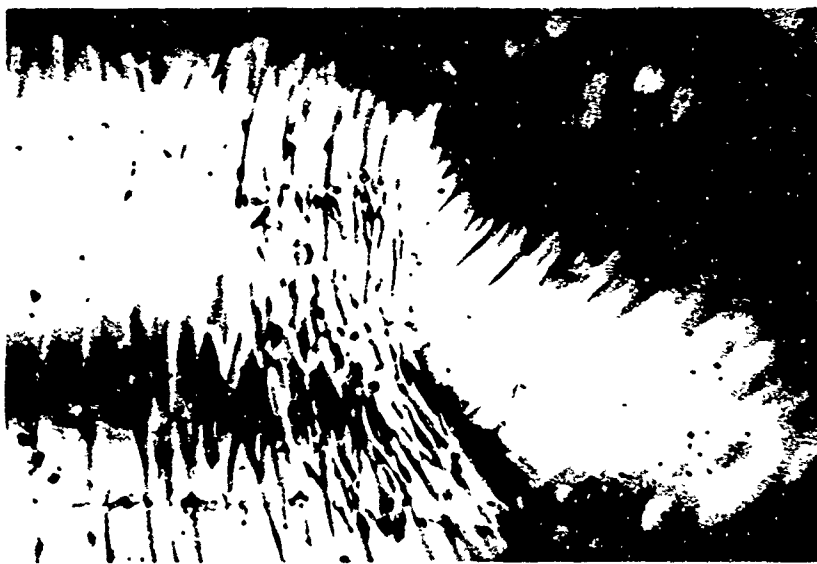


Fig. 10. Slip bands and microcracks in a U-10<sup>W/o</sup> Mo specimen exposed to pure, dry oxygen for 24 hours (600X).



Fig. 11. Coalescence of slip bands generating microcracks



Fig. 12. Intergranular cracks in a U-10<sup>w</sup>% Mo specimen exposed to pure, dry oxygen for 24 hours (800X).

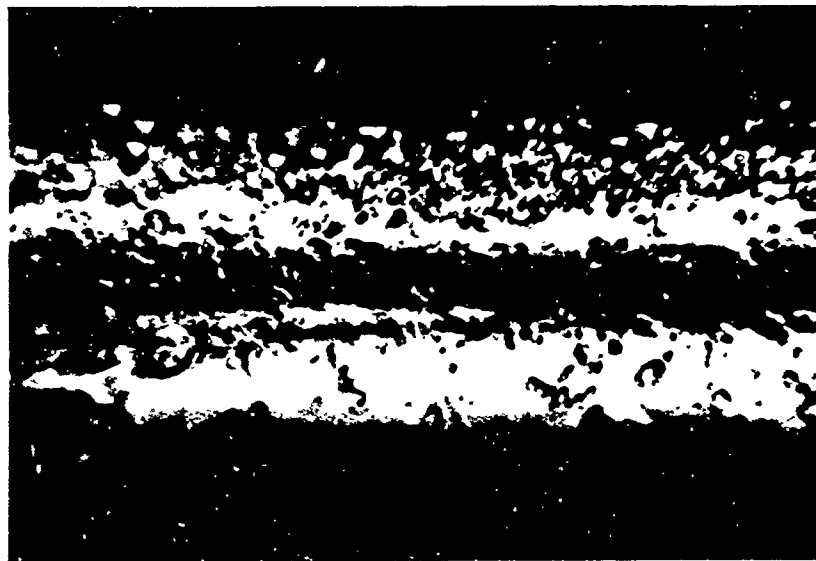


Fig. 13. Surface deterioration of a U-10<sup>w</sup>% Mo specimen exposed to wet oxygen (6 normalized partial pressure) (400X).



Fig. 14. Intersection of slip bands and concentration of corrosion products on a U-10<sup>w</sup>% Mo specimen exposed to wet oxygen (6 normalized partial pressure) (600X).



Fig. 15. Intergranular and transgranular cracks on a U-10<sup>v</sup>% Mo specimen exposed to wet oxygen (.6 mormalized partial pressure) (600X).

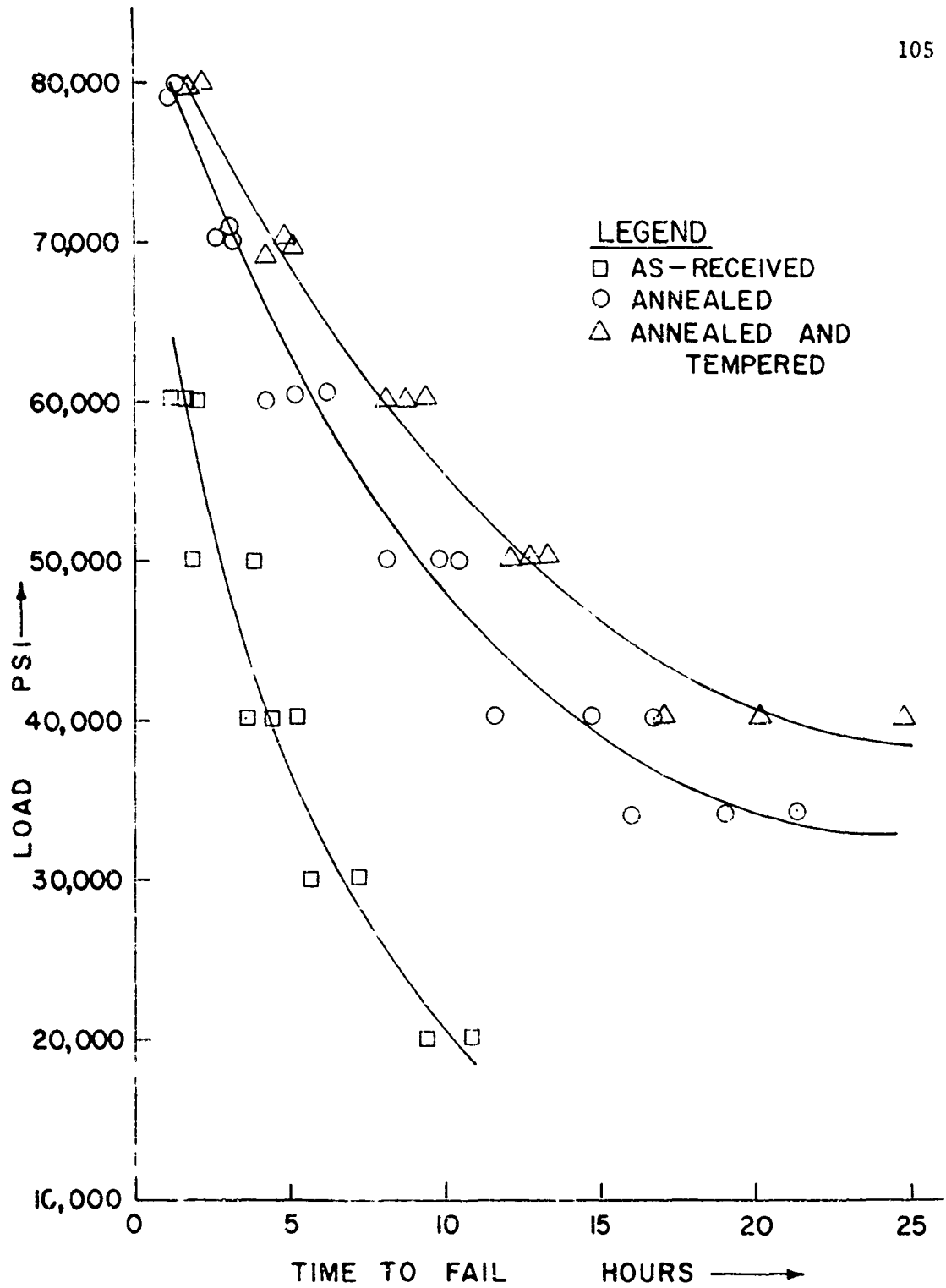


Fig. 16. Load vs. time to fail of U-10<sup>w</sup>% Mo specimens, "as-received" and heat treated.

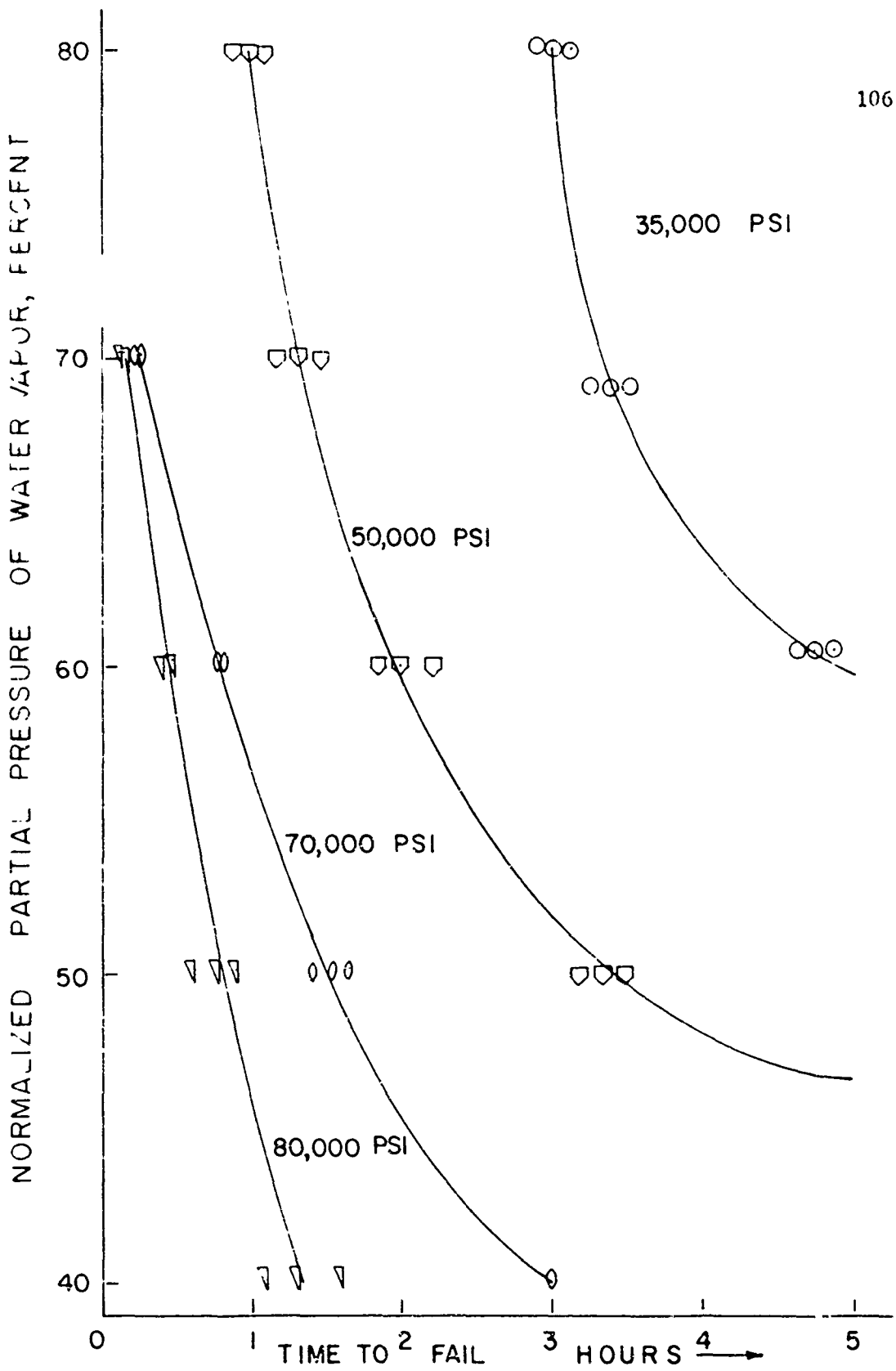


Fig. 17. Normalized partial pressure of water vapor vs. time to fail with tensile stress as a parameter.

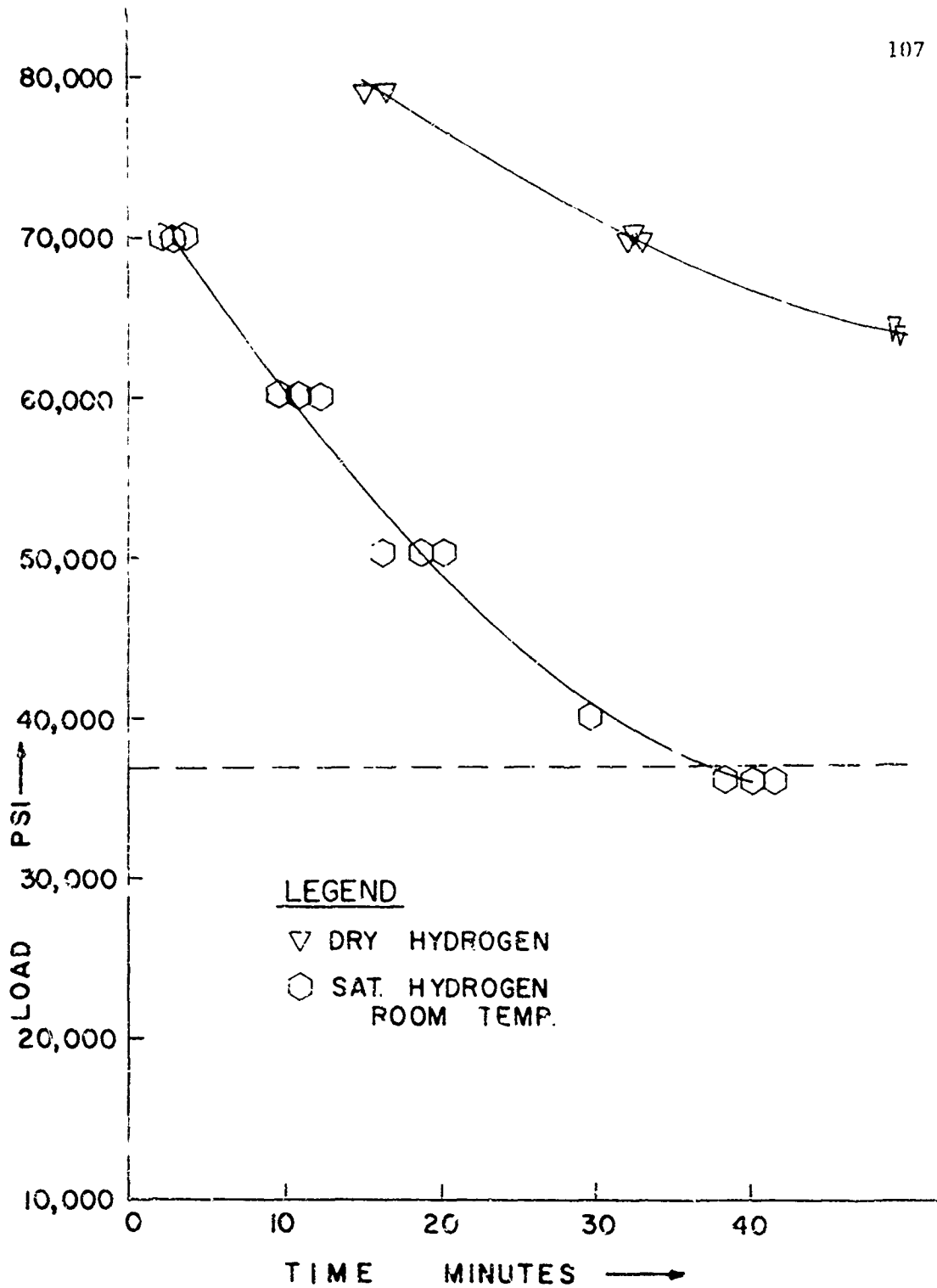


Fig. 18. Load vs. time to fail for U-10<sup>w</sup>o Mo specimens exposed to hydrogen both dry and saturated with water vapor at room temperature.

(a)



(b)



Fig. 19. Sequence of photomicrographs showing the process of fracture in a cyclically loaded specimen at intervals of 10 cycles. Specimen was loaded in dry, laboratory air.

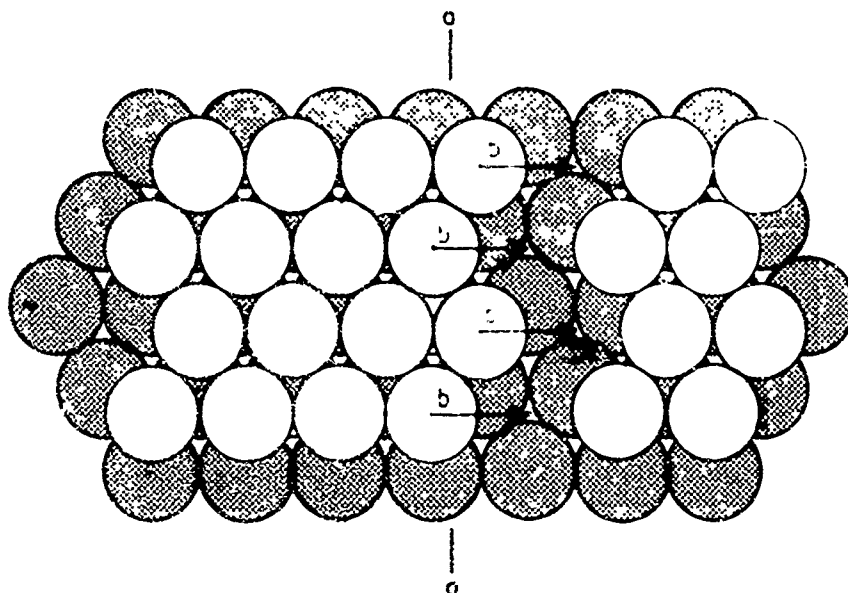


Fig. 20. A total dislocation (edge orientation) in a face-centered cubic lattice as viewed when looking down on the slip plane, after Reed-Hill (30).

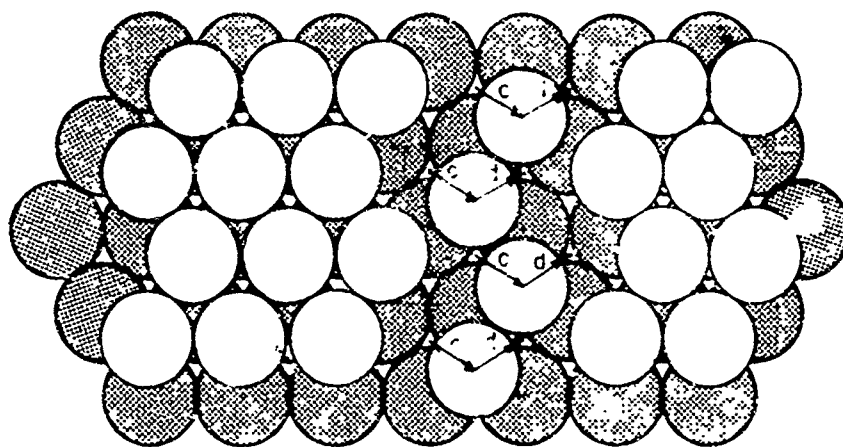


Fig. 21. Partial dislocation in a face-centered cubic lattice, after Reed-Hill (30).

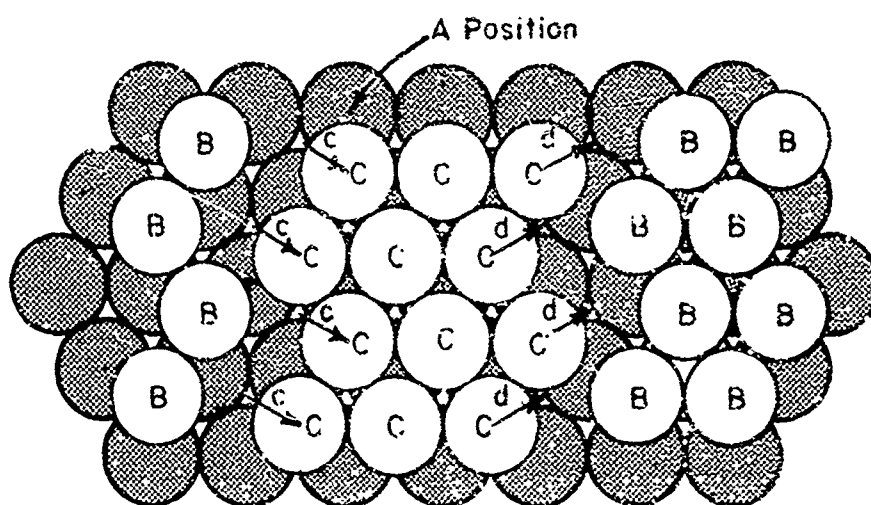


Fig. 22. An extended dislocation, after Reed-Hill (30).

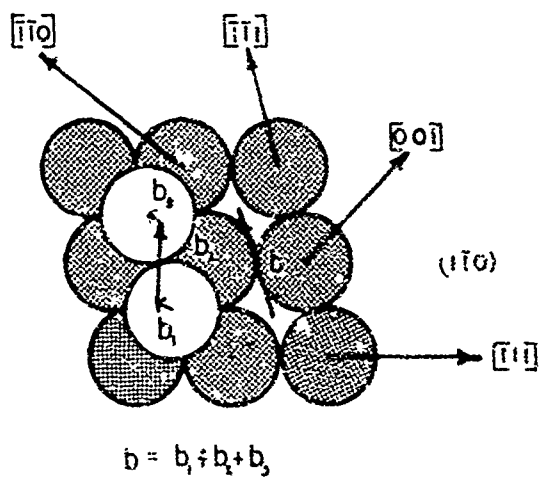


Fig. 23. The  $(1\bar{1}0)$  plane of the bcc lattice, after Weertman (28).

#### REFERENCES

1. Auxier, J. A., Health Physics, 11, 89 (1964).
2. Rienecker, F., and W. H. Moran, UCRL-12397 report on AEC Contract No. W-7405-eng-4k, Feb., (1965).
3. Pridgeon, J. W., Stress-Corrosion in Uranium-Molybdenum Alloys, Y-1417, Union Carbide Corporation, Nuclear Division, Plant Y-12, Oak Ridge, Tennessee, September, (1963), discussed in Ref. 2.
4. Creighton, D. L., Use of the Field-Emission Microscope in the Detection and Observation of Surface Cracks in Metals, Ph.D. Dissertation, The University of Arizona, (1964).
5. Creighton, D. L., and S. A. Hoenig, Trans. AIME, 233, 1368 (1965).
6. Avner, S. H., Introduction to Physical Metallurgy, McGraw-Hill Book Company, New York, (1964).
7. Polushkin, E. P., Defects and Failure of Metals, Elsevier Publishing Company, New York, (1956).
8. Uhlig, H. H., Physical Metallurgy of Stress-Corrosion Fracture, T. N. Rhodin, ed., Interscience Publishers, New York, (1959) 1-15.
9. Perryman, F. C. W., J. Inst. of Metals, 78, 621 (1950-51).
10. Mannheim, W. A., and H. K. Paxton, Report on ONR Contract No. 760 (14) NR G36-029, Carnegie Institute of Technology, Pittsburgh, Pennsylvania, AD 635 630, June, (1966).
11. Parkins, R. N., Met. Rev. The Inst. of Metals (GB), 9, (35), 201 (1964).
12. Edeleanu, C., Ibid. Ref. 8, 79-91.
13. Haynie, F. H., D. A. Vaughan, E. I. Phalen, W. K. Soyd, and P. D. Frost, AFML-TR-66-267, January, (1967).
14. Logan, H. L., Journal of Research of the National Bureau of Standards, 48 (2), 99 (1952).
15. Barnartt, S., Corrosion, 9, 322t (1962).

16. Mears, R., R. H. Brown, and E. Dix, Symposium on Stress-Corrosion Cracking of Metals, ASM-AIME, Philadelphia, (1945).
17. Bakish, R., and W. D. Robertson, J. Electrochem. Soc., 103, 320 (1956).
18. Dix, E. H., Trans. Inst. of Metals, AIME, 137, Techn. Publ. No. 1204 (1940).
19. Chaston, J. C., Nature (GB), 161, 891 (1948).
20. Hines, J. G., Corrosion Science, 1, 21 (1961).
21. Ehrlich, G., Annual Review of Physical Chemistry, 17, 295 (1966).
22. Huang, A. B., TDR No. AEDC-TDR-62-18, Air Force Systems Command, United States Air Force, January, (1962).
23. Swann, P. R., Scientific American, 214, 73 (1966).
24. Forty, A. J., Ibid. Ref. 8, 99-114.
25. Bergen, C. R., Corrosion, 20, (9), 269t (1964).
26. Thomas, K. C., and R. J. Allio, Nature (GB), 206, 82 (1965).
27. Dieter, G. E., Jr., Mechanical Metallurgy, McGraw-Hill Book Company, New York, (1961).
28. Weertman, J. and Julia R., Elementary Dislocation Theory, The Macmillan Company, New York, (1964).
29. Friedel, J., Dislocations, Pergamon Press, New York, (1964).
30. Reed-Hill, R. E., Physical Metallurgy Principles, D. Van Nostrand Company, Princeton, N. J., (1964).
31. American Institute of Physics Handbook, Second Edition, McGraw-Hill Book Company, New York, (1963), 2-190.
32. Kramer, I., and L. J. Demer, Progress in Materials Science, 9, (3), 133 (1961).
33. Coleman, E. G., D. Weinstein, and W. Rostoker, Acta. Met., 9, 491 (1961).
34. Tetelman, A. S., SU DMS Report No. 67-27, Dept. of Materials Science, Stanford University, Stanford, California, NASA CR 85771, July, (1967).

35. Sully, A. H., and W. A. Bell, J. Iron Steel Inst., 178, 15 (1954), discussed in Ref. 32.
36. Andrew, J. H., H. Lee, A. K. Malik, and A. G. Quarrell, J. Iron Steel Inst., 153, 67 (1946) discussed in Ref. 32.
37. Hann, G. L., A. R. Troiano, and E. C. Steigerwald, Trans. ASM, 57, 658 (1961).
38. Johnson, H. H., and A. M. Wilner, Appl. Matls. Res., 434, (1965).
39. Tetelman, A. S., and W. D. Robertson, Trans. AIME, 224, 775 (1962).
40. \_\_\_\_\_, Acta Met., 11, 415 (1963).
41. Bastien, P. G., Ibid. Ref. 8, 311-338.
42. Troiano, A., Trans. ASME, 52, 54 (1960).
43. Geuss, E., Surface Science, 2, 48 (1964).
44. Jastrzebski, Z. D., Nature and Properties of Engineering Materials, John Wiley and Sons, New York, (1959).
45. Metals Handbook, 8th Edition, ASM, Vol. 1, 999-1,000.
46. Swann, P. R., Corrosion, 19, (3), 102t (1963).
47. Groeneveld, T. P., E. E. Fletcher, and A. R. Elsea, N67-32396, Report on NASA Contract No. NAS 8-20029, June, (1967).
48. Hoke, J. H., AEC Report No. NYO-3257-1, on Contract No. AT(30-1)3257, June, (1965).
49. McHardy, J., Bureau of Naval Weapons Contract NOW 65-0327-f, Final Report, AD 633 767, February, (1966).
50. Jacobs, A. J., Naval Air System Command Contract No. NOW 66-0309d, Final Report, AD 813 396, May, (1967).
51. Beck, T. R., Boeing Scientific Research Laboratories, Seattle, Washington, AD 640 229, July, (1966).
52. \_\_\_\_\_, NASA Contract NAS 7-489, N67-28006, December, (1966).
53. Turley, R. V., C. H. Avery, and M. Sinclair, Technical Report No. AFML-TR-66-388, Air Force Materials Laboratory, December, (1966).
54. Humphries, T. S., NASA TY X-53483, June, (1966).

55. Allen, N. P., Fracture, B. L. Averback, D. K. Felbeck, G. T. Hahn, and D. A. Thomas, editors, The Technology Press, and John Wiley and Sons, New York, (1959), 123-145.
56. Orowan, L., Fatigue and Fracture of Metals, John Wiley and Sons, New York, (1952).
57. Hahn, G. T., B. L. Averback, W. S. Owen, and M. Cohen, Ibid. Ref. 56, pp. 91-116.
58. Stroh, A. N., Ibid. Ref. 56, pp. 117-122.
59. McClintock, F. A., J. Appl. Mech., 25, 282 (1958).
60. Uhlig, H. H. Discussion on S. Barnartt's paper, see Ref. 15.
61. Douglas, D. L., G. Thomas, and W. R. Roser, Corrosion, 20, (1), 15t (1964).
62. Thompson, D. H., Matls. Res. and Standards, 1, (2), 108 (1961).
63. Otte, H. M., JAP, 38, (1), 217 (1967).
64. Hoar, T. P., Corrosion, 20, (3), 109t (1964).
65. Mattson, E., Electrochim. Acta, 3, 279 (1961).
66. Peterson, C. A. W., and R. R. Vandervoort, UCRL-7767, report on AEC Contract No. W-7405-eng-48, Lawrence Radiation Laboratory, Livermore, California, March, (1964).
67. Ludwig, R. L. and J. W. Pridgeon, Y-1417, Union Carbide Corp., Nuclear Division, Plant Y-12, Oak Ridge, Tennessee, Progress reports 1 and 2, (1963).
68. Greenspan, J., AEC Report on "Delayed Cracking Behavior in U-8 Mo- 1/2 Ti and U-8 Mo alloys" April, (1962).
69. Ludwig, R. L., J. W. Pridgeon, and H. E. Patterson, Ibid. Ref. 67, Progress Report No. 3, (1963).
70. Private communication at ORNL, Oak Ridge, Tennessee, (1967).
71. Unpublished work on the "Effects of Static Electric D. C. Fields on the Stress-Corrosion Cracking of Alpha Brass in Ammonia", the Field Emission and Space Systems Laboratory, The University of Arizona, Tucson, Arizona.

72. Waber, J. T., manuscript prepared as a preprint for presentation at the Brussels Conference on the Aqueous Corrosion of Reactor Materials, work performed under the auspices of the US ALC, (1960).
73. Dwight, A. E., *J. Nuc. Mat.*, 2, 81 (1960).
74. Howlett, B. W., A. J. Eycott, I. K. Kang, and D. R. F. West, *J. of Nucl. Matls.*, 9, (2), 143 (1963).
75. Hoge, K. G., UCRL-12357, UC-25 TID-4500, February, (1965).
76. Gomer, R., *Field Emission and Field Ionization*, Harvard University Press, Cambridge, Mass., (1961).
77. Hoenig, S. A., *The Journal of Vacuum Science and Technology*, 3, (6), November/December, (1966).
78. Lundin, J. I., ORNL, private communication, (1967).
79. Cornett, M. H., NLCO-954, National Lead Company of Ohio, Cincinnati, Ohio, AEC Contract No. AT(30-1)-1156, March, (1966).
80. Woods, K. N., L. E. Smith, and R. D. Leggett, BNWL-30, Pacific Northwest Laboratory, Richland, Washington, January, (1965).
81. McGregor Tegart, W. J., *The Electrolytic and Chemical Polishing of Metals in Research and Industry*, Pergamon Press, New York, (1959).
82. Gorman, E. F., "Inert Gases for Controlled-Atmosphere Process", Reprinted from the *Welding Journal*, September, (1958).
83. *Handbook of Chemistry and Physics*, Chemical Rubber Publishing Co., (1960), Table of the Physical Constants of Inorganic Compounds, p. 678.
84. Kramer, D., and C. G. Rhodes, *Trans. of Met. Soc. of AIME*, 224, 1015 (1962).
85. Chirigos, J. N., *Ibid.* Ref. 8, 70-78.
86. Childs, L. L., and F. E. Evans, RFP-816, report on AEC contract No. AT(29-1)-1106, The Dow Chemical Company, Rocky Flats Division, Golden, Colorado, December, (1966).
87. Tetelman, A. S., and T. L. Johnston, *Phil. Mag.*, 11, 389 (1965).
88. Brick, R. M., B. R. Gordon, and A. Phillips, *Structure and Properties of Alloys*, McGraw-Hill Book Company, New York, (1965).

89. Hull, D., Introduction to Dislocations, Pergamon Press, New York, (1965).
90. Cohen, J. B., R. Hinton, K. Lay, and S. Sass, *Acta Met.*, 10, 894 (1962).

DOCUMENT CONTROL DATA - R & D

(Security classification of title, body of abstract and indexing annotation must be entered when the overall report is classified)

1. ORIGINATING ACTIVITY (Corporate author) Arizona Board of Regents The University of Arizona Aerospace - Mechanical Engineering Department Tucson, Arizona		2a. REPORT SECURITY CLASSIFICATION Unclassified	
		2b. GROUP	
3. REPORT TITLE A FIELD-EMISSION MICROSCOPE INVESTIGATION OF THE EFFECTS OF AMBIENT ATMOSPHERES ON THE STRESS-CORROSION CRACKING OF URANIUM-MOLYBDENUM ALLOYS			
4. DESCRIPTIVE NOTES (Type of report and inclusive dates) Final Report			
5. AUTHOR(S) (First name, middle initial, last name) Herman Sulsona			
6. REPORT DATE March 1968		7a. TOTAL NO. OF PAGES 117	7b. NO. OF REFS 90
8a. CONTRACT OR GRANT NO. DA-18-001-AMC-1063(X)		9a. ORIGINATOR'S REPORT NUMBER(S)	
8b. PROJECT NO. AMCMS Code 5910.21.61026		9b. OTHER REPORT NO(S) (Any other numbers that may be assigned this report)	
8c.			
8d.			
10. DISTRIBUTION STATEMENT This document has been approved for public release and sale; its distribution is unlimited.			
11. SUPPLEMENTARY NOTES		12. SPONSORING MILITARY ACTIVITY U.S. Army Ballistic Research Laboratories Aberdeen Proving Ground, Maryland	
13. ABSTRACT The effects of heat treatment and ambient atmospheres on the stress-corrosion cracking behavior of U-10 w/o Mo were investigated using a field-emission microscope of cylindrical geometry. Cathodic protection and the effect of static electric DC fields were investigated as possible protective techniques in the stress-corrosion cracking of U-10 w/o Mo. A special "gas shield" protective technique was also investigated. The stress-corrosion cracking behavior of U-10 w/o Mo was found to be influenced by heat treatments. A gamma homogenization and quench followed by a tempering treatment were found to be most beneficial in reducing the susceptibility of the alloy. A tentative "critical stress" for initiation of stress-corrosion cracking was set at 36,500 psi. This critical stress was found to be strongly dependent upon heat treatments and internal structure. Cracking of U-10 w/o Mo in specific atmospheres was found to be either intergranular, transgranular or both, depending on the particular atmosphere. Intergranular cracking was found to be promoted by increasing the water vapor content of the atmosphere. U-10 w/o Mo was found to be susceptible to hydrogen embrittlement. Cathodic protection and electric fields had no effect on the stress-corrosion cracking behavior of U-10 w/o Mo. Pure, dry nitrogen on the other hand, was found to be most effective as a protective shield during cyclic loading of U-10 w/o Mo specimens.			

14. KEY WORDS	LINK A		LINK B		LINK C	
	ROLE	WT	ROLE	WT	ROLE	WT
Metals						
Alloys						
Uranium Alloys						
Uranium-Molybdenum Alloys						
Reactors						
Pulse Nuclear Reactors						
Bare Metal Nuclear Reactors						
Nuclear Reactor Fuels						
Mechanical Properties						
Corrosion						
Stress Corrosion						
Stress Corrosion Cracking						
Fracture						
Brittle Fracture						
Ductile Fracture						
Intergranular Cracking						
Transgranular Cracking						
Hydrogen Embrittlement Effects						
Gas-Water Vapor Atmospheric Effects						
Gaseous Atmospheric Effects						
High Temperature Properties						
Heat Treatments						
Field Emission Microscopy						
Cathodic Protection						
Static Electric DC Field Effects						

END

6/27/68